11 Trapped Ions and Atoms

Among the first of the systems that were suggested for building a quantum computer was a linear trap with stored atomic ions. Atomic ions have some attractive properties for use as qubits: qubits can be defined in ways that make decoherence very slow while simultaneously allowing for readout with high efficiency. To avoid perturbing these ideal properties, the ions are best isolated in space. This can be achieved with electromagnetic traps, which arrange electric and magnetic fields in such a way as to create a potential minimum for the ion at a predetermined point in space. Similarly, neutral atoms can be trapped in the electromagnetic field of a standing light wave.

Lasers are an extremely important part of experiments with single ions and atoms. They are used for

- Generating gate operations
- Reading out the results
- Initializing the qubits
- Cooling the motional degrees of freedom
- Trapping neutral atoms.

11.1 Trapping ions

11.1.1 Ions, traps and light

Earnshaw's theorem states that static electromagnetic fields cannot trap a charge in a stable static position[1]. However, using a combination of static and alternating electromagnetic fields it is possible to confine ions in an effective potential.

[1] In the purely electrostatic case the existence of a minimum of the electrostatic potential in a charge-free region would violate Gauss' law. See for a discussion of Earnshaw's theorem in a modern context.

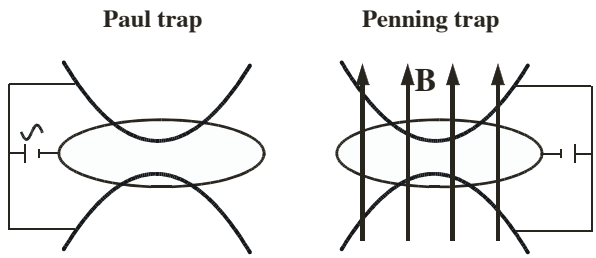

Figure 11.1: Two classical ion traps.

Figure 11.1 shows schematically the geometries used in the two traditional traps, the Paul and Penning traps. Both consist of an axially symmetric set of electrodes. The electrodes on the symmetry axis have the same potential, while the ring has the opposite polarity. The resulting field is roughly that of a quadrupole, where the field vanishes at the center and increases in all directions.

In the case of the Paul trap, the voltage on the electrodes varies sinusoidally: The electrodes generate a potential

$$\Phi(x,y,t) = (U - V\cos(\omega t))\frac{x^2 - y^2}{2r_0^2}.$$

The ion is therefore alternately attracted to the polar end caps or to the ring electrode. On average, it experiences a net force that pushes it towards the center of the trap. In the exact center, the field is zero and any deviation results in a net restoring force. The Penning trap has the same electrodes, but the electric field is static: it is repulsive for the end caps. The ions are prevented from reaching the ring electrode by a longitudinal magnetic field.

11.1.2 Linear traps

The Paul Trap can also be made into an extended linear trap. Figure 11.2 shows the geometry used in this

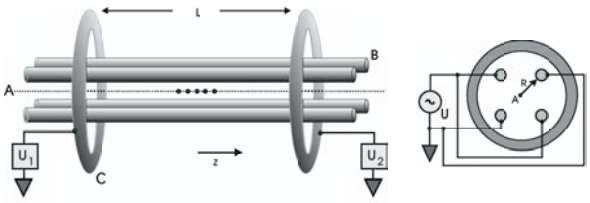

Figure 11.2: Linear quadrupole trap.

design, which consists of four parallel rods that generate a quadrupole potential in the plane perpendicular to them. The quadrupole potential is alternated at a radiofrequency, and the time-averaged effect on the ions confines them to the symmetry axis of the trap, while they are free to move along this axis. A static potential applied to the end caps prevents the ions from escaping along the axis. The resulting effective potential (averaged over an rf cycle) can be written as

$$V = \omega_x^2 x^2 + \omega_y^2 y^2 + \omega_z^2 z^2,$$

where ω_α, $\alpha = x, y, z$ are the vibrational frequencies along the three orthogonal axes. By design, one has $\omega_x = \omega_y \gg \omega_z$, i.e., strong confinement perpendicular to the axis and weak confinement parallel to the axis.

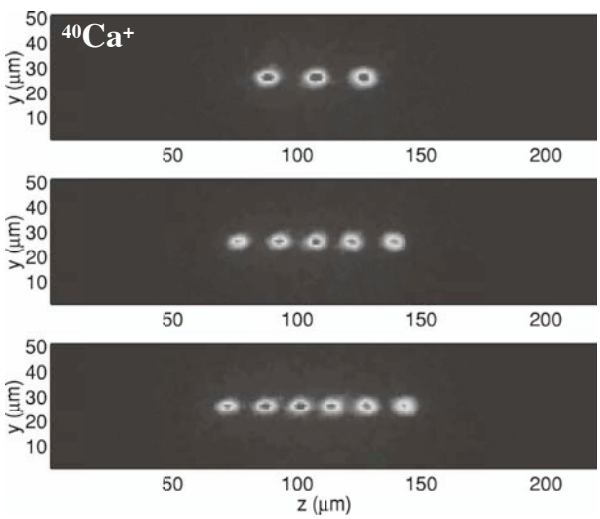

Figure 11.3: Strings of ions in linear traps.

Ions that are placed in such a trap will therefore preferentially order along the axis. The distance between the ions is determined by the equilibrium between the confining potential $\omega_z^2 z^2$ and the Coulomb repulsion between the ions. This type of trap has two important advantages for quantum computing applications: it allows one to assemble many ions in a linear chain where they can be addressed by laser beams and the equilibrium position of the ions (on the symmetry axis) is field-free. This is in contrast to the conventional Paul trap where the Coulomb repulsion between the ions pushes them away from the field-free point. As a result, two or more ions in a Paul trap perform a micromotion driven by the rf potential. In the linear Paul trap, the field-free region is a line where a large number of ions can remain in zero field and therefore at rest.

When more than one ion is confined in such a trap, the system has multiple eigenmodes of the atomic motion. The lowest mode is always the center of mass motion of the full system, in analogy to the motion of atoms in a crystal. A change of the fundamental vibrational mode can be compared to the Mössbauer effect, where the recoil from the photon is shared between all atoms in the crystal. The higher vibrational modes, which correspond to phonons with nonzero wave vector, as well as the vibrational modes that include wave vector components perpendicular to the axis, will not be relevant in this context.

11.2 Interaction with light

The interaction of light with atomic ions is essential for building a quantum computer on the basis of trapped ions: it is used for initializing, gating, and readout. We therefore discuss here some of the basics of the interaction between light and atomic ions.

11.2.1 Optical transitions

When light couples to atomic ions, the electric field of the optical wave couples to the atomic electric dipole moment:

$$\mathscr{H}_e = -\vec{E} \cdot \vec{\mu}_e,$$

where $\vec{E}$ is the electric field and $\vec{\mu}_e$ the atomic electric dipole moment. For the purpose of quantum information processing applications, it is important to distinguish between “allowed" and “forbidden" optical transitions. In the first case, the matrix element of the electric dipole moment operator for the transition is of the order of 10^{-29} C m; in the latter, it is several orders of magnitude smaller.

The size of the electric dipole moment determines not only the strength of the interaction with the laser field and thus the ease with which the ion can be optically excited, it also determines the lifetime of the electronically excited states. According to Einstein's theory of absorption and emission, the spontaneous emission rate is proportional to the square of the matrix element. States that have an optically allowed transition to a lower lying state are therefore unsuitable for use in quantum computers, since the associated information decays too fast.

While an atom has an infinite number of energy levels, it is often sufficient to consider a pair of states to discuss, e.g., the interaction with light. Writing $|g\rangle$ for the state with the lower energy (usually the ground state) and $|e\rangle$ for the higher state, the relevant Hamiltonian can then be written as

$$\mathscr{H}_{2LS} = -\omega_0 \mathbf{S}_z - 2\omega_1 \cos(\omega t)\mathbf{S}_x.$$

Here, $\hbar\omega_0 = E_e - E_g$ is the energy difference between the ground and excited state and $2\omega_1\cos(\omega t)$ is the coupling between the laser field (with frequency ω) and the atomic dipole moment. The operators $\mathbf{S}_x$ and $\mathbf{S}_z$ are pseudo-spin-1/2 operators.

If the Hamiltonian is written in this way, the analogy to the real spin-1/2 system, as was discussed in Chapter 10, is obvious. This allows us to treat two-level transitions as virtual spins-1/2 [145]. In the interaction representation with respect to the laser frequency, the coordinate system “rotates" at the laser frequency ω around the z-axis of the virtual spin. Neglecting the counter-rotating component at frequency $2\omega_1$, we get the effective Hamiltonian

$$\mathscr{H}^r_{2LS} = -(\omega_0 - \omega)\mathbf{S}_z - \omega_1 \mathbf{S}_x, \tag{11.1}$$

in close analogy to the rotating frame representation of NMR (see section 10.1.3). In optics, this is known as the *rotating wave approximation*.

11.2.2 Motional effects

When an atom is not at rest, its transition frequency is shifted through the Doppler effect:

$$\omega = \omega_0 + \vec{k}\cdot\vec{v},$$

where $\vec{k}$ is the wave vector of the laser field and $\vec{v}$ the atomic velocity. In free atoms, the velocity can have arbitrary values, with the probability of a specific velocity determined by the Boltzmann distribution. The optical spectra of ensembles of atoms are therefore broadened and/or shifted according to their motional state.

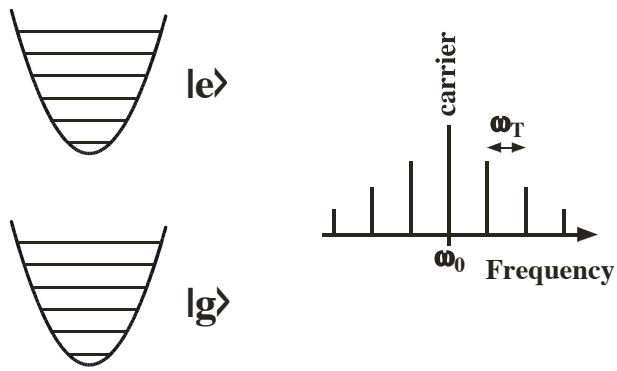

Figure 11.4: Energy levels of the trapped atom (left) and the resulting spectrum (right).

In trapped ions, the motional energy is quantized. Depending on the trap potential, the motional states can often be approximated by a collection of harmonic oscillators. Harmonic oscillator motion does not shift the frequency by arbitrary amounts, but creates sidebands that are separated from the carrier frequency ω_0 by the harmonic oscillator frequency. As shown in Figure 11.4, the trap motion creates a set of sidebands whose frequencies can be written as $\omega_n = \omega_0 + n\omega_T$, where $-\infty < n < \infty$ is the order of the sideband and ω_T is the trap frequency. Since every motional degree of freedom creates such a sideband pattern, the resulting spectrum can contain a large number of resonance lines.

In all techniques suggested to date, for quantum computing with trapped ions, the spatial coordinates of the qubit ions play an important role either as a qubit or as a variable used for coupling different

qubits. If the spatial degrees of freedom are used in the computation, the motional state of the ion must be well controlled and initialized to a specific state, which is usually the motional ground state. The ions must therefore be cooled into their ground state as a part of the initialization process [170].

11.2.3 Basics of laser cooling

The technique to bring them into the ground state is laser cooling, which was developed in the 1980's [171, 172, 173, 174, 175, 176]. It relies on the transfer of momentum from photons to atoms during an absorption (and emission) process. Suitable arrangements allow one to use this momentum transfer to create extremely strong forces that push the atoms in the direction of the laser beam. Adjusting the experimental parameters properly, these forces can be conservative (i.e., they form a potential) or they can be dissipative friction forces. Conservative forces are useful for logical gate operations, while frictional forces are useful for initialization and cooling.

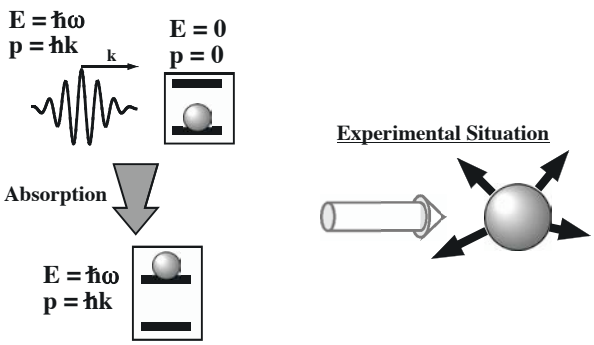

Figure 11.5: Photon momentum as the source of mechanical effects of light.

The origin of these mechanical effects of light can be traced to the momentum $\hbar k$ that every photon carries. As shown in Figure 11.5, the photon momentum is transferred to the atom whenever a photon is absorbed. During the subsequent spontaneous emission process, the recoil of the photon emission also contributes to the mechanical effects of the light on the atom. However, the emission is, in contrast to the absorption process, not directed. The average effect of all emission processes therefore vanishes.

The momentum change due to the transfer of a single photon momentum is relatively small; it corresponds to a change in the atomic velocity of a few cm/s. As an example, we calculate the momentum transferred by a single photon at a wavelength of 589 nm, a prominent wavelength in the spectrum of Na:

$$\Delta p = \frac{h}{\lambda} = \frac{6.626 \cdot 10^{-34}\text{Js}}{589 \cdot 10^{-9}\text{m}} = 1.125 \cdot 10^{-27}\frac{\text{m kg}}{\text{s}}.$$

Given the mass $m_{\text{Na}} = 3.818 \cdot 10^{-26}$ kg of the sodium atom, this corresponds to a change in its velocity of

$$\Delta v = \frac{\Delta p}{m_{\text{Na}}} = 2.95\frac{\text{cm}}{\text{s}}.$$

This estimate was first made by Einstein in 1917 [177] and verified experimentally by Frisch 1933 [178] with a classical light source. Since the atoms scattered less than three photons in his experiment, the effect was very small.

However, if an allowed atomic transition is excited by a laser, the atom re-emits the photon within a few nanoseconds (16 ns for Na) and is ready to absorb another photon. It can therefore scatter up to 10^8 photons per second, and the momentum transferred by them adds up to a force

$$F = \frac{\Delta p}{\tau} = \frac{1.125 \cdot 10^{-27}\frac{\text{m kg}}{\text{s}}}{\text{ns}} = 7.03 \cdot 10^{-20}\text{N},$$

corresponding to an acceleration of

$$\begin{aligned} a &= \frac{F}{m_{\text{Na}}} = \frac{7.03 \cdot 10^{-20}\text{N}}{3.82 \cdot 10^{-26}\text{kg}} \\ &= 1.84 \cdot 10^{6}\frac{\text{m}}{\text{s}^2} = 188\,000\,g. \end{aligned}$$

This implies that an atom arriving with the velocity of a jet plane can be stopped over a distance of a few centimeters.

In the case of trapped ions, the situation may also be discussed in terms of resolved motional sidebands. Cooling is then achieved by irradiating the lower-frequency sidebands, as shown in Figure 11.6. In reality, the laser drives not only the $|g,3\rangle \leftrightarrow |e,2\rangle$ transition, but all $|g,n\rangle \leftrightarrow |e,n-1\rangle$ transitions for $n > 0$.

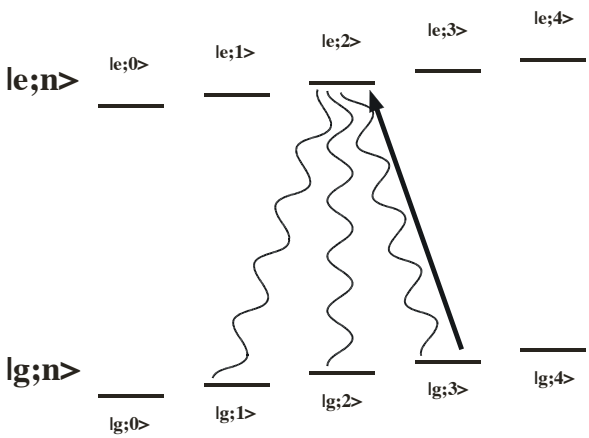

Figure 11.6: Schematics of sideband cooling for a single degree of freedom.

For each absorption event, the vibrational quantum number is reduced by one unit, since the photon energy is smaller than the energy difference of the two internal states. The emission process occurs with roughly equal probabilities into the different ground states, thus not affecting the average vibrational energy. The only state that is not coupled to the laser is the $|g,0\rangle$ state, since no transition with a frequency below the carrier originates from this state. As a result, all atoms eventually are driven into this state in the absence of heating mechanisms.

11.3 Quantum information processing with trapped ions

Cold trapped ions were among the first candidates for qubits (see, e.g., [179]), but it took several years of intense experimental work to realize this potential [180].

11.3.1 Qubits

Since the atomic ions stored in traps have a large number of states, there are many distinct possibilities for defining qubits. Since spontaneous decay times through allowed transitions are of the order of a few nanoseconds, the requirement of long decoherence times implies that both states of the qubits must either be sublevels of the electronic ground state or metastable states, i.e., states where all transitions to lower lying states are “forbidden".

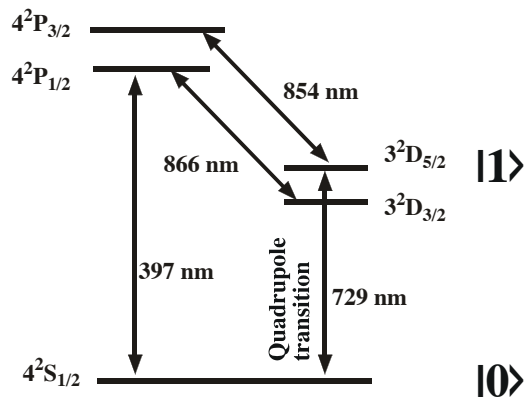

Figure 11.7: Possible qubit implementation using a metastable state in Ca^+.

A typical example of a a qubit implementation is the Ca^+ ion [181]. In its ground state [Ar](4s), the single valence electron is in the 4s orbital, which is abbreviated by the term symbol $4^2S_{1/2}$. If the electron is excited into a 3d orbital, it has angular momentum $L = 2$, and can only decay to the ground state by emitting two quanta of angular momentum. These quadrupole transitions are “forbidden" in the dipole approximation, resulting in long lifetimes of the excited state. Nägerl *et al.* [182] therefore suggested using the transition between the $4^2S_{1/2}$ ground state and the $3^2D_{5/2}$ excited state as a qubit.

Apart from the computational basis states, the ion has many other states that cannot be completely omitted. In particular, the $3^2D_{3/2}$ state is important, since it can be populated and also has a long lifetime. To bring it back into the qubit system, the 866 nm transition to the $4^2P_{1/2}$ state can be driven with an additional laser. From there, the ions quickly decay to the ground state.

The second common choice is to encode the quantum information in sublevels of the electronic ground state [183, 184]. Figure 11.8 shows as an example the possible encoding of a qubit in the hyperfine levels of the electronic ground state of Be^+. The two qubit states correspond to the $|F = 2, m_F = 2\rangle$ and $|F = 1, m_F = 1\rangle$ hyperfine states. Since the

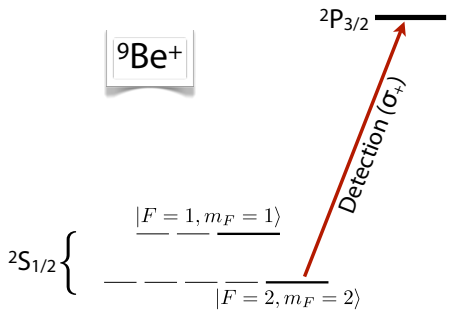

Figure 11.8: Possible qubit implementation using two hyperfine states of $^9Be^+$.

spontaneous transition rate between ground states is very small, the lifetime is again long compared to all relevant timescales. The transitions from the two ground state hyperfine levels to the electronically excited state $^2P_{1/2}$ are sufficiently well resolved to allow one to optically distinguish whether the ion is in the $|2,2\rangle$ or $|1,1\rangle$ state.

The initialization of the qubits must bring the ion into a specific internal state as well as into the motional ground state. While the laser cooling for the initialization of the external state was described above, the initialization of the internal state can be achieved by optical pumping. The principle of optical pumping is very similar to sideband cooling: a laser drives the system in such a way that only the desired state of the ion does not couple to the laser, while ions in other states can absorb light, become excited and return to an arbitrary sublevel of the ground state. These absorption / emission cycles are repeated until the ion falls into the state that does not couple. Given enough time, all ions will therefore assemble into the uncoupled state. In this case, the dissipative process that is required for the initialization step is spontaneous emission.

11.3.2 Single-qubit gates

The way to generate (pseudo-)spin rotations that correspond to single qubit gates depends on the specific choice of the qubit states. If the two states encoding the qubit are connected by an optical transition, it is possible to apply laser pulses that have the same effect as RF pulses acting on spin qubits. The corresponding Hamiltonian (11.1) has the same structure as that of a spin-1/2. Since the spatial separation of the ions is typically of the order of 10 optical wavelengths, it is possible to use tightly focused laser beams aimed at individual ions to separately address the qubits [14]. While the optical transitions used for such qubits must be “forbidden", the tightly focused laser beams that are required for addressing qubits individually provide sufficiently high Rabi frequencies for efficient excitation.

If the qubit is defined by two hyperfine states that are connected by a magnetic dipole transition, the situation is even more directly related to magnetic resonance. In this case, the transition between the two qubit states is a magnetic dipole transition, which can be driven by microwave fields [185]. Since the wavelength of microwave radiation is large compared to the distance between the ions, microwaves will interact with all qubits simultaneously. Addressing of individual qubits therefore requires a magnetic field gradient to separate the transition frequencies of the ions.

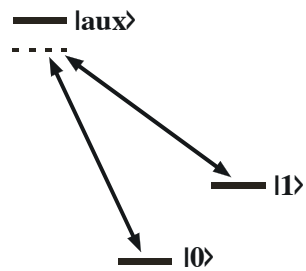

Figure 11.9: Raman excitation of a hyperfine qubit.

The second possibility for addressing hyperfine qubits is to use Raman laser pulses. For this purpose, one uses two laser fields [186], whose frequency difference matches the energy level separation of the two qubit states. The laser frequency is close to a transition to an auxiliary state. Choosing an appropriate set of parameters (frequencies, field strengths), it is possible to generate laser pulses that effectively drive the transition between the two qubit states, with negligible excitation of the auxiliary state [183].

11.3.3 Two-qubit gates

Two-qubit gates that can form the basis of a universal quantum computer, require, in addition to the single-qubit operations, an interaction between qubits. In the case of trapped ions, the main interaction is the Coulomb repulsion between neighboring ions, which are separated by a few micrometers in typical traps. This interaction can be utilized for two-qubit operations in different ways, depending on the qubit implementation.

The Coulomb repulsion between the ions couples their motional degrees of freedom. As in a solid, the motion of ions in a trap is best described in terms of eigenmodes that involve all ions. This quantized motion is often involved in quantum information processing. Initial demonstrations of quantum information processing used the lowest two states of the harmonic oscillator as a qubit [183], and other implementations and proposals involve them as an intermediate bus-qubit.

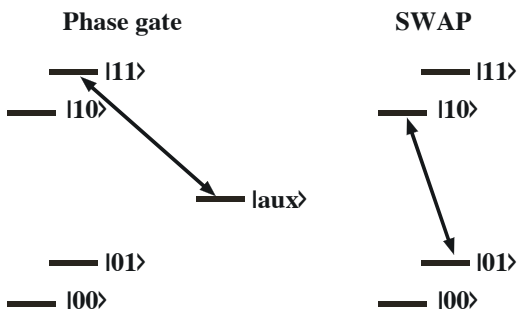

Figure 11.10: Selective laser pulse to generate a phase shift of state $|11\rangle$ (left) and a SWAP operation (right).

We therefore first discuss a two-qubit gate that uses the internal degrees of freedom of a $^9Be^+$ ion as the target qubit and the harmonic oscillator motion as the control qubit of a CNOT gate [183]. Figure 11.10 shows two examples of simple two-qubit gates that can be realized by such a scheme. The notation $|\alpha\beta\rangle$ refers to the internal state α and the motional state β.

In the first example, resonant radiation that couples only the state $|11\rangle$ to an auxiliary state executes a 2π pulse. As in any two-level system, the two-level system consisting of $|11\rangle$ and $|\text{aux}\rangle$ acquires a phase $e^{i\pi} = -1$ by the pulse. Since the other states are not affected, the overall effect of the pulse on the computational basis states is

$$P_4 = \begin{pmatrix} 1 & 0 & 0 & 0 \\ 0 & 1 & 0 & 0 \\ 0 & 0 & 1 & 0 \\ 0 & 0 & 0 & -1 \end{pmatrix}.$$

This phase gate can be combined with two $\pi/2$ pulses into a CNOT operation [183]. Another important two-qubit gate, the SWAP operation, can be generated by a π pulse on the red sideband (see Figure 11.10).

While motional degrees of freedom are not ideal as actual qubits, they appear to be useful for executing two-qubit gates between ions: A two-qubit gate between ions j and k is executed by first swapping the information from ion j into the oscillator mode, executing the two-qubit gate between oscillator and ion k, as described above, and subsequently swapping the information from the oscillator back to ion j. Since the harmonic oscillator motion involves all ions, this procedure works for any pair of ions, irrespective of their distance.

11.3.4 Readout

One of the important advantages of trapped ion quantum computers is the possibility of optically reading out the result with a very high selectivity and success probability. A photon from a laser focused to an ion and tuned to an allowed optical transition is absorbed with almost 50

$$probability and the photon is re-emitted after typically$$

, however, this is still not sufficient. It is therefore necessary to repeat the absorption-emission process several thousand times to obtain an unambiguous signature of the state of the qubit. These repetitions must be performed without chaning the state of the qubit. This can be achieved is the laser frequency is tuned to an optical cycling transition from the state that is to be detected, focuses it on the ion to be measured, and detects the fluorescence emitted.

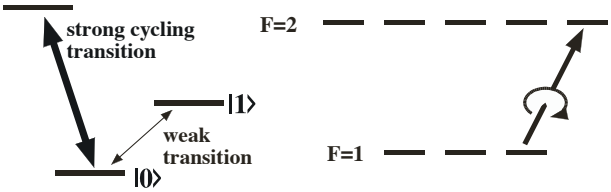

Figure 11.11: Optical readout of a single qubit: the left-hand part shows the relevant states and transitions, the right-hand part an example of a cycling transition.

The term “cycling transition" means that the state to which the ion is excited can only fall back to the particular ground state from which it was excited. Figure 11.11 shows an example of such a cycling transition between an electronic state with total angular momentum $F = 1$ and a second state with $F = 2$. If circularly polarized light couples to the $|F = 1, m_F = 1\rangle$ ground state, it excites the atom into the $|F = 2, m_F = 2\rangle$ excited state. The selection rule $\Delta m_F = \pm 1$ does not allow for transitions to any ground state but the $|F = 1, m_F = 1\rangle$ state.

For suitable transitions, up to 10^8 photons can be scattered. If the detection system has a 1% collection efficiency, this yields a very reliable decision whether the ion is in the particular state or not.

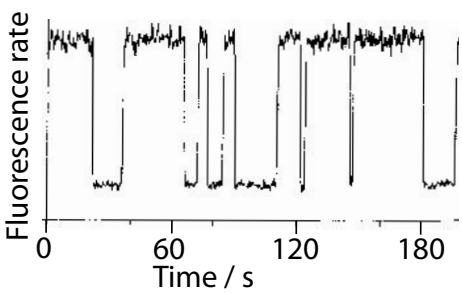

Figure 11.12: Fluorescence of a single Ba ion. The quantum jumps indicate changes of the internal quantum state of the ion [187].

Figure 11.12 shows an example for an observed signal [187]: when the single Ba ion is in the observed state, it scatters approximately 2200 photons per second; the background rate is less than 500 photons per second. As shown in the example data, the fluorescence level is an excellent indicator if the ion is in the state that is being measured. The sudden drops in the fluorescence level indicate that the ion jumps into a different state, which is not coupled to the transition being irradiated. These transitions are referred to as “quantum jumps" .

The detection scheme sketched here only provides a measure of the atom being in state $|0\rangle$; a similar measurement of state $|1\rangle$ is only possible if that state is also part of a cycling transition. The complementary measurement of the atom being in state $|1\rangle$ can be achieved in different ways. The first possibility is to take the absence of a result for the state $|0\rangle$ measurement as a measurement of the atom being in state $|1\rangle$. This is possible since the system (under ideal conditions) *must* be either in state $|0\rangle$ or state $|1\rangle$. A second possibility is to perform first the measurement of state $|0\rangle$ and then apply a logical NOT operation and a second measurement of state $|0\rangle$. Since the NOT operation interchanges the two states, a subsequent measurement of the state $|0\rangle$ is logically equivalent to a measurement of state $|1\rangle$ before the NOT operation.

11.4 Experimental implementations

11.4.1 Systems

One of the most popular ions for quantum information studies is the Ca^+ ion [182, 94]. For laser cooling, excitation of resonance fluorescence and optical pumping of the ground state, different transitions are used. The experiment therefore requires laser sources at the wavelengths 397 nm, 866 nm, and 854 nm. If the E2 transition between the ground state and the metastable $D_{5/2}$ state is used as the qubit, a fourth laser with a wavelength of 729 nm is required. Its frequency stability must be better than 1 kHz.

The long lifetimes make hyperfine ground states very attractive for quantum information processing applications. Examples for such systems are the $^{171}Yb^+$[185] and $^9Be^+$ ions [186].

The linear Paul trap was mostly used for quantum information processing, but some variants are also

being tested. Tight confinement of the ions is advantageous as it increases the separation between the vibrational levels and therefore facilitates cooling into the motional ground state. In addition, the vibrational frequencies are involved in the logical operations. Accordingly higher vibrational frequencies imply faster clocks.

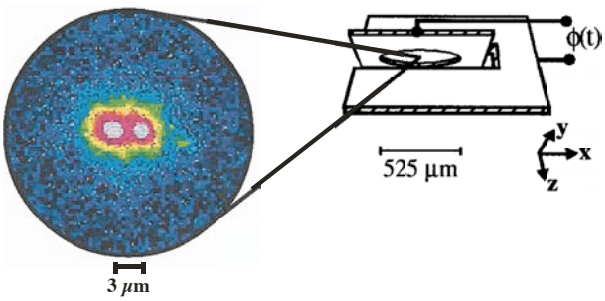

Figure 11.13: Two ions in a small elliptical trap [170].

Tight confinement can be achieved mainly by miniaturization of the traps. For the example shown in Figure 11.13, the smallest trapping frequency is 8.6 MHz [170]. However, miniaturization is not without difficulties: it increases, e.g., the effect of uncontrolled surface charges in the trap and it makes addressing of the ions more difficult.

11.4.2 Some results

The earliest quantum logic operation was reported by the group of Wineland [183]. They used a $^9Be^+$ ion where one of the qubits was a pair of internal states, two hyperfine sublevels of the electronic ground state, the $|F=2,m_F=2\rangle$ and $|F=1,m_F=1\rangle$ states with an energy difference of 1.25 GHz. This qubit represented the target qubit. The control qubit was defined by the two lowest harmonic oscillator states, which were separated by 11 MHz. A sequence of three Raman pulses was used to implement a CNOT gate.

Figure 11.14 shows the populations of the four possible states of the system before (front row) and after (back row) the application of the CNOT gate. The control qubit, which is shown in white, does

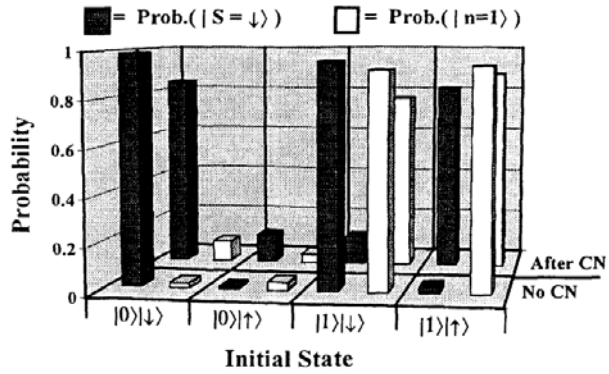

Figure 11.14: Experimental test of the CNOT gate on single $^9Be^+$ ion [183].

not change during the CNOT operation. The target qubit, shown in black, remains also roughly constant when the control qubit is in the $|0\rangle$ state (shown in the first two columns) but changes when the control is 1 (3^{rd} and 4^{th} column).

Other achievements with this system include cooling of two ions into the vibrational ground state and their entanglement [170, 186]. For this purpose the authors did not address the ions individually, but modified the effective Rabi frequency through fine-tuning of their micromotion. The resulting state was not a singlet state (but close to it) and the scheme is not directly applicable to quantum computing.

Using Ca^+ ions in a linear trap, optical addressing of individual ions was demonstrated [188], and in a chain of three ions, coherent excitation of ions [189].

The two-qubit Cirac–Zoller gate[127] was realized on two trapped Ca^+ ions [14] by tuning the laser to a blue-shifted sideband, where, in addition to the electronic transition of the given ion, the collective motion of the two ions was also excited. Single-qubit gates were realized by a laser beam whose frequency was resonant with the quadrupole transition and which was focused so tightly that it interacted only with a single ion. The final state was measured by exciting the S–P transition of the trapped ions and measuring the fluorescence. Since the ions can only be excited when they are in the S state, high fluorescence counts are indicative of the qubit being in the $|0\rangle$ state.

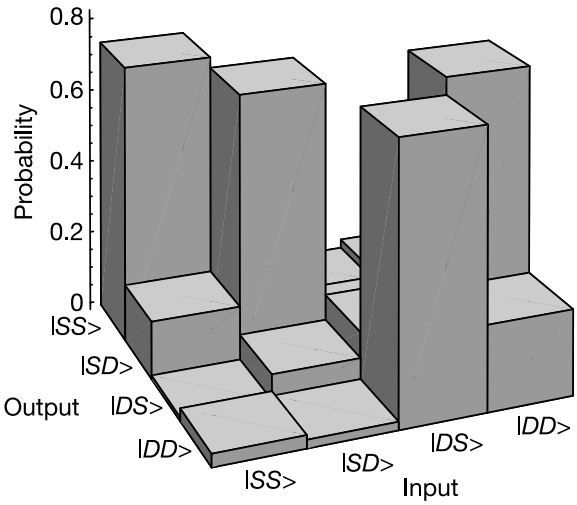

Figure 11.15: CNOT gate implemented on two trapped Ca^+ ions [14].

A two-qubit gate has also been implemented on two trapped beryllium ions by Leibfried *et al.* [15]. They used two hyperfine states of the electronic ground state to store the quantum information. In this experiment, the motion of the ions was excited by two counterpropagating laser beams, whose frequencies differed by 6.1 MHz. As a result, the ions experience a time-dependent effective potential that resonantly excites the oscillatory motion in the trap. The parameters of the excitation were chosen such that the ions were not directly excited, but instead their quantum states were transported around a closed loop in parameter space. As shown by Berry [190], the parameters of such a circuit can be chosen in a way that the transported states acquire a net phase. Leibfried *et al.* used this procedure to implement a phase gate on their system. Since the laser beams interact with both ions, additional lasers will be required for generating specific single-qubit gates in this system. In a similar system, a Grover-type search was implemented [191].

While these demonstration experiments were done on a small number of ions, proposals exist how the number of ions could be scaled up, particularly by integrating the trap electrons on a chip [117]. Operation of such a microfabricated trap was demonstrated for a single ion [192].

11.4.3 Challenges

One of the biggest problems of ion traps is that the ions, as charged particles, are relatively sensitive to stray fields in the vicinity. These fields can adversely affect the motion of the ions and, if they are time dependent, they heat the ions. Typical heating times are of the order of 1 ms [170] for two ions in a trap. With increasing numbers of ions, heating rates are expected to increase so that not only the number of particles that couple to these stray fields, but also the number of degrees of freedom that can be driven, increases.

Like all other implementations of quantum computers, ion traps will have to demonstrate that they can perform a sufficiently large number of gate operations. As the number of ions in a trap increases, it becomes more and more difficult to control the ions. In particular, the trap frequency (i.e. the confinement) decreases, while the number of motional modes increases and heating effects become more effective. It appears thus unlikely that individual traps will be able to accept a sufficiently large number (i.e., hundreds) of ions.

Several solutions to this problem have been proposed, such as storing the ions in multiple traps. It has been suggested [193] that it should be possible to couple these separate traps through photons, thus creating an arbitrarily large quantum register with a linear overhead. As a first step towards this goal, quantum interference between two remote trapped $^{174}Yb^+$ ions was reported [194]. A similar approach is the so-called quantum charge-coupled device (QCCD), a microfabricated array of electrodes that can trap the ions and shift them around between "interaction-" and "memory-"regions [117].

Addressing of qubits by lasers must be achieved in the far-field diffraction-limited regime, where the separation between the ions must be large compared to an optical wavelength. This requirement sets a lower limit on the distance between the ions and therefore on the strength of the axial confinement potential. Since this potential also determines the vibrational frequency that enters the clock speed, it is obvious that ion traps cannot be operated with arbitrary speed. While direct microwave pulses

can distinguish between the ions through their frequency separation in an inhomogeneous magnetic field [185], it is not clear that this will allow for significantly tighter confinement.

11.5 Neutral atoms

Neutral atoms can also be used as qubits [195]. Compared to trapped ions, they offer potentially lower decoherence rates, since their interactions with the environment are weaker. For the same reason, neutral atoms are more difficult to trap, store and manipulate.

11.5.1 Trapping neutral particles

The first prerequisite for using neutral atoms as qubits is a means to control their position and velocity. Since electrostatic forces cannot be used, one has to resort to electromagnetic waves that interact with the induced dipole moment of the atoms and / or to magnetic fields that interact with the static magnetic dipole moment of the atoms.

For quantum computing applications, the main tool for generating mechanical forces acting on atoms are laser beams. The effect can be understood in simple terms by considering the potential energy surface generated by the laser field. Starting from the classical expression for the energy of an electric dipole μ_e in an electric field E,

$$U = -\vec{E} \cdot \vec{\mu}_e,$$

we calculate the force acting on the atom as

$$F = -\vec{\nabla} U = \vec{\nabla}(\vec{E} \cdot \vec{\mu}_e).$$

In the absence of saturation, the induced dipole moment $\vec{\mu}_e$ increases linearly with the strength of the field, $\vec{\mu}_e \propto \vec{E}$, and the potential is thus proportional to the square of the field strength.

The sign of the potential depends on the difference between the laser frequency and the atomic transition frequency: For a red-detuned laser (i.e. laser frequency smaller than the transition frequency), the

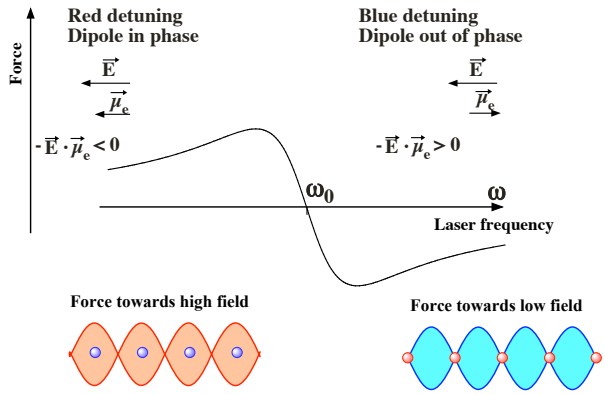

Figure 11.16: Effect of laser-detuning with respect to the optical resonance frequency: for a red-detuned laser, the atomic dipole oscillates in phase with the laser field and the atoms are pulled into the high field region. For a blue-detuned laser, the induced dipole is out of phase and the atoms are pushed out of the areas of high laser intensity.

atomic dipole oscillates in phase with the laser field, $\vec{\mu}_e \cdot \vec{E} > 0$ and the energy becomes negative. In this case, the atom is pulled into the region of maximal field, where its potential energy is minimal. In the case of a blue-detuned laser, the atomic dipole is out of phase with respect to the field, the energy becomes positive and the atom is pushed out of the high-field region.

A simple example of a laser-based trap for neutral particles is a tightly focused laser beam. Such traps were initially used for the manipulation of neutral atoms, but also for macroscopic particles [196, 174, 197]. The depth of the trap (i.e. the maximum kinetic energy that a particle can have without escaping from the trap) is determined by the laser intensity and the detuning of the laser frequency from the atomic resonance: the strength of the induced dipole moment decreases linearly with the frequency difference. While it would therefore be advantageous to tune the laser close to the resonance, this would also cause absorption. In the context of quantum information processing, however, absorption of light from the trapping laser must be avoided since this would cause decoherence. One therefore uses a

large detuning and high laser intensity.

A suitable geometry for trapping neutral atoms for quantum computing is a standing wave generated by superimposing two counterpropagating laser beams. This generates a linear sequence of potential minima, separated by half of the laser wavelength. Another possibility is an array of tightly focused laser beams [198, 199]. To make such a scheme scalable, the different foci can be generated by microlenses, either in one or two dimensions [200].

11.5.2 Manipulating neutral particles

A trap can be filled, e.g., by placing it directly in a sample of cold atoms. However, such a process will always generate a random filling of the different minima of the trap, which is not compatible with the requirements of quantum information processing. If the traps are small enough, the interaction between the atoms reduces the probability of filling the trap with more than one atom [201]. In an array of such traps, a parameter range exists, in which an ensemble of cold atoms will preferentially occupy every microtrap with a single atom [202]. This regime is called a Mott insulator state and may be used to create quantum registers if the separation between the microtraps is in a range suitable for the separation of qubits.

If the separation between the microtraps is smaller than the required distance between the qubits or if the fluctuations of the populations are too large, active control of the populations is required. For a linear trap, this was demonstrated experimentally [203, 204] by combining the trapping laser with a second standing wave trap, at a right angle to the quantum register.

For these experiments, it is necessary to shift the trap potential. This can be achieved in one dimension by shifting the phase of the counterpropagating laser beams that form the standing wave [205]. Shifting the phase of one beam by ϕ shifts the standing-wave pattern, i.e. the trap potential, by

$$\delta = \phi \frac{\lambda}{4\pi},$$

where λ is the laser wavelength. If the phase shift is time-dependent, i.e. realized by a frequency shift of one of the laser beams, this results in a linear motion of the trap potential. Acceleration can be implemented by a frequency chirp.

Laser-optical traps are in general state-selective: depending on the internal state of the atom, the interaction can be strong or weak, and the atoms can be confined to or expelled from regions of high laser intensity. This effect must be taken into account when gate operations are applied that change the internal state of the atoms. The state-selectivity can also be used, to specifically manipulate subsets of the atoms that are in specific internal states.

11.5.3 Gate operations

Single qubit gate operations can be performed on neutral atoms in much the same way as on atomic ions, using laser pulses with appropriate wavelength and polarization. The qubit states will typically be hyperfine sublevels of the electronic ground state. Transitions between them can be excited either by Raman laser pulses or by microwave pulses [206, 207].

For two-qubit operations, a state-dependent interaction must be present between the different qubits. In contrast to trapped ions, neutral atoms do not experience Coulomb forces. They can, however, interact by electric or magnetic dipole couplings, which depend on their internal state. This interaction is of course significantly weaker than the Coulomb interaction, and has a shorter range. Nevertheless, it appears possible to use these interactions, and the shorter range may even prove beneficial, since it reduces unwanted long-range interactions.

The strength of the interaction between qubits can be controlled, e.g., via the distance between them. This required independent trapping of two subensembles, e.g. by using two dipole traps with different polarizations, such that one trap represents the dominant interaction for atoms in one internal state, while the orthogonal polarization dominates for the other state [208]. The two potentials have the same periodicity but are displaced with respect to each other, and

the displacement may be controlled. Thus, atoms in different spin states may be brought into contact with each other in a well-defined way and for a well-defined time. If the time-dependence of the interaction is properly adjusted, the overall effect of such a controlled collision between cold atoms generates an entangling quantum logical gate operation [209, 210]. The strength of the interaction and therefore the speed of the gate operations can be increased significantly if the atoms are briefly promoted to a highly excited Rydberg state [211].

Another possibility for controlling the coupling between atoms is to bring them into optical resonators. If two atoms interact with the same resonator mode, they experience an indirect interaction with each other [212]. Alternatively, the atoms can be put into separate optical resonators, which are then coupled to each other, e.g. through an optical fiber [193]. These schemes involve some degree of population of electronically excited states. Accordingly, a major challenge for their implementation is the need to avoid spontaneous emission, which destroys the quantum coherence in these systems.

11.6 Interacting atoms in optical lattices

In a pioneering experiment, Greiner et al [202], following a theoretical suggestion of Jaksch et al. [213], observed a "quantum phase transition from a superfluid to a Mott insulator in a gas of ultracold atoms", as the title of the paper says. The paper demonstrated for the first time that it is possible to construct physical realizations of theoretical models for condensed-matter systems with adjustable values of the model parameters and without many of the complications present in real-world condensed-matter systems. A lot of activity followed, both experimental and theoretical. The phenomena and the tools employed in their study have been discussed in a number of reviews of varying level, perspective, and length [214, 215, 216, 217, 218].

Atoms in optical lattices thus are excellent illustrations of Feynman's [4] concept of using quantum systems to simulate other quantum systems. It also seems possible to construct gates, initialize qubits and perform other operations essential for the implementation of universal quantum computation. A significant drawback, however, remains the lack of individual adressability of the atoms stored in an optical lattice.

11.6.1 Interacting particles in a periodic potential: The Hubbard model

For a discussion of the Hubbard model, we need a few basic notions from the theory of crystalline condensed matter. In ordinary solids the electrons move in a periodic potential generated by the ion charges. The interaction between electrons is often neglected or treated implicitly in some form of effective-field approximation unless it is absolutely necessary to proceed otherwise. The interatomic distances in a solid are of the order of the atomic radius, which leads to overlap between electronic wavefunctions of neighboring atoms, to chemical bonding, and, under suitable conditions, to the ability of electrons to move around in the crystal. In an "artificial solid" of atoms in an optical lattice this is different: the lattice constant (the distance between neighboring potential wells) is given by the light wavelength, $\lambda_L \approx 10^{-6}$m, much larger than the typical size of an atom, about 10^{-10}m. All short-range variations in the interatomic potential can thus be neglected when we discuss effects of the interatomic interactions in an optical lattice. Furthermore, the electrons in a real solid are inevitably spin-1/2 fermions, whereas an optical lattice can be populated with either bosonic or fermionic atoms.

Before discussing interatomic interaction effects, however, we have to understand the behavior of a single atom (or, equivalently, of a number of non-interacting atoms) in a D-dimensionally periodic potential of the form

$$V(\vec{r}) = V_0 \sum_{i=1}^{D} \sin^2 k_L r_i. \tag{11.2}$$

The potential is generated by superposing D standing-wave laser beams of wavenumber $k_L =$

$2\pi/\lambda_L$ in orthogonal directions, thus creating a simple cubic (or square, or one-dimensional) lattice of potential minima with lattice constant $a = \lambda_L/2$. The potential strength V_0 is given by the intensity of the laser beam. As the intensity varies avross the beam, (for example in a Gaussian shape with maximum intensity in the center of the beam), V_0 should be considered weakly position-dependent. In addition, V_0 may also vary along the beam due to focusing effects. The spatial variation of V_0, though necessary to keep the atoms from moving out of sight, will be neglected.

The motion of a free particle is completely characterized by the momentum $\vec{p} = \hbar\vec{k}$, and the particle's wave function is a plane wave

$$\psi_{\vec{k}}(\vec{r}) = \frac{1}{\sqrt{\Omega}} e^{i\vec{k}\cdot\vec{r}}, \tag{11.3}$$

where Ω is a normalization volume. The energy of the particle is

$$\varepsilon_{\vec{k}} = \frac{\hbar^2 k^2}{2m}. \tag{11.4}$$

In an optical lattice the laser frequency is tuned to be roughly (but not precisely) euqal to a transition frequency of the atom; the emission or absorption of a photon will thus be accompanied by a kinetic energy of recoil

$$E_R = \frac{\hbar^2 k_L^2}{2m}. \tag{11.5}$$

A periodic potential acting on a free particle changes both wave function and energy. Instead of a plane wave (11.3) the wave function becomes a modulated plane wave, or Bloch function,

$$\psi_{\vec{k}}(\vec{r}) = u_{\vec{k}}(\vec{r}) e^{i\vec{k}\cdot\vec{r}}, \tag{11.6}$$

where the function $u_{\vec{k}}(\vec{r})$ (the "Bloch factor") has the periodicity of the potential $V(\vec{r})$ (11.2). The dispersion relation (energy-momentum relation) $\varepsilon_{\vec{k}}$ (11.4) changes gradually as the potential strength is slowly increased. For very weak potential $\varepsilon_{\vec{k}}$ essentially keeps its free-particle form (11.4); however, it turns out to be convenient to write it in the form

$$\varepsilon_{\vec{k},\vec{g}} = \frac{\hbar^2}{2m}(\vec{k}+\vec{g})^2, \tag{11.7}$$

where $\vec{g}$ is a vector of the reciprocal lattice, defined by requiring that the plane waves $e^{i\vec{g}\cdot\vec{r}}$ have the periodicity of the lattice (or the potential $V(\vec{r})$). In the simple cubic case, all components of every $\vec{g}$ are integer multiples of $\frac{2\pi}{a} = \frac{4\pi}{\lambda_L}$. In the dispersion (11.7) $\vec{k}$ is then restricted to the first Brillouin zone, the region of reciprocal space ($\vec{k}$ space) closer to $\vec{g} = \vec{0}$ than to any other $\vec{g}$. In the simple cubic case that is the cube $[-\pi/a, \pi/a]^3$. In $\varepsilon_{\vec{k},\vec{g}}$ then $\vec{g}$ classifies different branches of the dispersion relation, leading to different energy bands . The lowest energy band obviously is the one with $\vec{g} = \vec{0}$. At the Brillouin zone boundary, for example at $\vec{k} = (\pi/a, 0, 0)$, the $\vec{g} = \vec{0}$ and $\vec{g} = (-2\pi/a, 0, 0)$ bands are degenerate. Degenerate perturbation theory shows that the degeneracy is lifted by a weak potential V_0. The formerly degenerate energy levels are pushed away in opposite directions and an energy gap is created. The set of energy bands and gaps is called the band structure, and is an important means in understanding the behavior of crystalline condensed matter; compare, for example [219, 220] for details. Note that for sufficiently weak potential strength V_0 the maximum energy of the lowest band is of the order of

$$\frac{\hbar^2}{2m}\left(\frac{\pi}{a}\right)^2 = \frac{\hbar^2}{2m}\left(\frac{2\pi}{\lambda_L}\right)^2 = \frac{\hbar^2 k_L^2}{2m} = E_R. \tag{11.8}$$

The bandwidth of the lowest energy band for "nearly free" particles is thus equal to the recoil energy (11.5).

The Hamiltonian for non-interacting fermions or bosons in an optical lattice can now be written in the occupation number (or "second quantization") formalism:

$$\mathbf{H} = \sum_{\vec{k},\vec{g}} \varepsilon_{\vec{k},\vec{g}} c^\dagger_{\vec{k},\vec{g}} c_{\vec{k},\vec{g}}\,, \tag{11.9}$$

where $c^\dagger_{\vec{k},\vec{g}}$ ($c_{\vec{k},\vec{g}}$) is the creation (annihilation) operator for a particle in a single-particle energy eigenstate with quantum numbers $\vec{k}$ and $\vec{g}$. The operator $n_{\vec{k},\vec{g}} = c^\dagger_{\vec{k},\vec{g}} c_{\vec{k},\vec{g}}$ is the occupation number operator for that eigenstate. (Note that the Bloch functions $\psi_{\vec{k}}$ and the Bloch factors $u_{\vec{k}}$ in (11.6) should also bear $\vec{g}$ or some other appropriate band index as $\vec{k}$ is restricted to the first Brillouin zone.)

Let us now discuss the effects of interatomic interactions in an optical lattice. Since typical interatomic distances are comparable to λ_L and thus very large compared to atom sizes, the interatomic potential essentially only acts through its long-range part which can be parametrized in terms of the scattering length a_S:

$$V_{\rm int}(\vec{r}-\vec{r}') = \frac{4\pi\hbar^2}{m} a_S \delta(\vec{r}-\vec{r}'). \tag{11.10}$$

In order to treat this short-range potential, it is convenient to use a basis set of localized single-particle wave functions instead of the Bloch functions (11.6) extending over the whole "crystal". This basis set is given by the Wannier functions [219, 220]

$$w_n(\vec{r}-\vec{l}) = \frac{1}{\sqrt{N}} \sum_{\vec{k}} e^{-i\vec{k}\cdot\vec{l}} \psi_{n\vec{k}}(\vec{r}). \tag{11.11}$$

Here, N is the number of lattice sites $\vec{l}$ in the system (equal to the number of $\vec{k}$ vectors in the first Brillouin zone) and n is an index indicating the band of interest. (Labeling bands by the reciprocal lattice vectors $\vec{g}$ is convenient only close to the free-particle case.) Each Wannier function is centered around a lattice site $\vec{l}$, and decays with growing distance from $\vec{l}$. If the potential wells of the optical lattice are very deep and well separated from each other (that is, for large V_0) the Wannier functions for the lowest energy bands are the lowest energy eigenstates of a single potential well (similar to orbitals of an isolated atom), and the Bloch functions are linear combinations of atomic orbitals.

Denoting the creation and annihilation operators for particles in a Wannier state by $c^\dagger_{\vec{l}n}$ and $c_{\vec{l}n}$, respectively, the Hamiltonian of non-interacting particles may be written as

$$\mathbf{H} = \sum_{\vec{l},\vec{l}'} t_{\vec{l}-\vec{l}'n} c^\dagger_{\vec{l}n} c_{\vec{l}'n}, \tag{11.12}$$

where the "hopping elements" $t_{\vec{l}-\vec{l}'n}$ are given by

$$t_{\vec{l}-\vec{l}'n} = \frac{1}{N} \sum_{\vec{k}} \varepsilon_{\vec{k}n} e^{i\vec{k}\cdot(\vec{l}-\vec{l}')}. \tag{11.13}$$

Indices labeling spin or other internal degrees of freedom have been suppressed. The formal expression (11.13) for the hopping elements can be rewritten in terms of the Wannier functions at lattice sites $\vec{l}$ and $\vec{l}'$. For the large-V_0 case the Wannier functions are well localized within each potential minimum and the hopping elements will be negligible except for $\vec{l}$ and $\vec{l}'$ nearest neighbors. If the Wannier functions are isotropic, all nonvanishing hopping elements will have the same value, which we call $-t_n$. The non-interacting particles then are described by the energy bands

$$\varepsilon_{\vec{k}n} = -2t_n \sum_{i=1}^{D} \cos k_i a. \tag{11.14}$$

In the same spirit, the interaction between atoms via the potential (11.10) can be discussed. The interaction term of the Hamiltonian then contains a sum of terms, each with four electron creation and annihilation operators and an integral involving Wannier functions located at four lattice sites. From the localization properties of the Wannier functions it is then clear that the dominant term is the one where all Wannier functions are located at the same lattice site. Neglecting all other terms, the interaction is given by the single value

$$U = \frac{4\pi\hbar^2}{m} a_S \int d^3r\, |w_n(\vec{r})|^4. \tag{11.15}$$

Since we focus on a single band, the band index n can be omitted. The total Hamiltonian depends on the statistics of the atoms involved. If the atoms are spin-half fermions (with internal quantum number $\sigma = \uparrow, \downarrow$) we obtain the Hubbard model [221, 222, 223] in its original form

$$\mathbf{H} = -t \sum_{\vec{l},\vec{l}',\sigma} c^\dagger_{\vec{l}\sigma} c_{\vec{l}'\sigma} + U \sum_{\vec{l}} n_{\vec{l}\uparrow} n_{\vec{l}\downarrow} \tag{11.16}$$

($\vec{l},\vec{l}'$ nearest neighbors), where $n_{\vec{l}\sigma} := c^\dagger_{\vec{l}\sigma} c_{\vec{l}\sigma}$ is the number operator. The model (11.16) and its many extensions are popular in solid-state physics for modeling the electron correlation effects believed to be important in magnetism, metal-insulator transitions, and high-temperature superconductivity. If the atoms are bosons (all in the same internal atomic state) the Hamiltonian is known as the bosonic Hubbard model

$$\mathbf{H} = -t \sum_{\vec{l},\vec{l}'} c^\dagger_{\vec{l}} c_{\vec{l}'} + \frac{U}{2} \sum_{\vec{l}} n_{\vec{l}}(n_{\vec{l}} - 1), \tag{11.17}$$

originally [224] employed to describe superfluids in porous media or granular superconductors.

In contrast to the situation in real-world condensed matter systems modelled by Hubbard-type Hamiltonians, the parameter values t and U for atoms in an optical lattice can be easily tuned by varying the laser field strength V_0 in (11.2). If V_0 increases, the potential wells get steeper and narrower and the wave functions get compressed, so that U (11.15) increases. Approximating the potential well by a D-dimensional paraboloid and the wave function by the appropriate oscillator ground state, one obtains $U \sim V_0^{D/2}$.

→ **Problem**

By the same mechanism the overlap between wave functions in neighboring potential wells will decrease as V_o grows, and hence the nearest-neighbor hopping amplitude t will decrease exponentially. The ground-state properties of the Hubbard model depend only on the ratio U/t and thus on the laser field strength V_0.

11.6.2 (Observing) The Mott-Hubbard transition

In the experiment of Greiner et al. [202] ultracold bosonic ^{87}Rb atoms were trapped in an optical lattice produced by a laser with $\lambda_L = 852$nm. The recoil energy (11.8) then is $E_R \approx k_B \cdot 0.15\mu$K and the trapping potential was $V_0 \lesssim 22E_R$. Non-interacting free ($V_0 = 0$) bosons at zero temperature will condense into the lowest plane-wave state (11.3), with $\vec{k} = \vec{0}$. The situation does not change decisively if a weak interatomic interaction and a weak lattice potential are present: the state remains a macroscopically coherent (superfluid) many-boson state.

With growing strength of the lattice potential V_0, the single-particle states become progressively localized and the repulsive interaction U dominates the Hamiltonian (11.17) more and more. If the total number of particles is small enough, every lattice site (or potential well) contains at most one atom. For strong enough V_0 each atom will be strongly localized in one potential well and will not enjoy enough overlap to its neighbors to develop long-range phase coherence of the wave function. If every potential well contains exactly one atom[2], further atoms can only be added at the price of an excitation energy U per atom. The same energy gap also prevents the formation of doubly occupied sites (and accompanying vacancies) which would be needed to achieve particle transport. The resulting state is obviously incompressible and, thinking in terms of the original (electronic) Hubbard model, insulating. Therefore it is known as the Mott (-Hubbard) insulator state.

The transition between the superfluid and Mott insulating states was demonstrated in a time-of-flight experiment [202]. For small or moderate potential strength V_0 all bosons convene in the lowest-energy extended Bloch state in a coherent manner. As the Bloch state is a periodically modulated plane wave (11.6) it contains Fourier components with different $\vec{g}$ values, with $\vec{g} = \vec{0}$ dominating as V_0 goes to zero. In the experiment the optical potential is switched off suddenly and the atoms are allowed to expand freely. The Fourier components with different $\vec{g}$ separate spatially according to their different propagation speeds. After a fixed expansion time an absorption image is taken. The absorption images of Figure 11.17 therefore map directly the distribution of the atoms in reciprocal space.

For free atoms, ($V_0 = 0$) the lowest-energy Bloch state is an unmodulated $\vec{k} = \vec{0}$ plane wave. The corresponding absorption image in Figure 11.17.a therefore shows a single spot in the center. As V_0 grows, additional Fourier components enter the lowest Bloch state and become visible in the absorption image, which develops into a two-dimensional projection of the reciprocal lattice (Figure 11.17 b,c,and d). However, upon further growth of V_0 the reciprocal lattice spots fade away again, their intensity being soaked up by a big central blob. That blob (Figure 11.17 g and h) is witness to the fact that the state has evolved into one where each potential minimum houses one atom, with no phase relation between neighboring atoms and hence no interference visible. The large extent of the central absorption spot in reciprocal space reflects the localization of each

[2] The situation is similar for any other integer number of atoms per site.

atom in real space. This shows clearly the change in the nature of the ground state as the ratio U/t is varied. The expected change in the nature of the low-energy excitation spectrum from gapless in the superfluid state to gapped in the Mott insulating state could also be observed [202] by analyzing tunneling between neighboring potential wells which are energetically displaced with respect to each other in an applied external field.

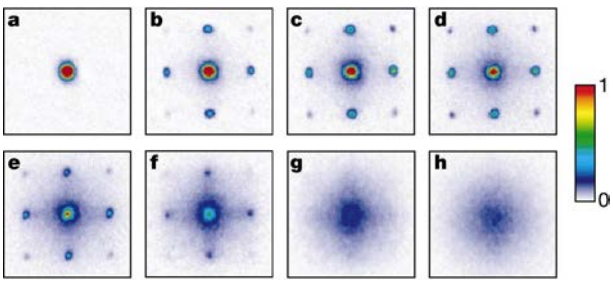

Figure 11.17: Absorption images reflecting the Fourier component structure of the many-particle wave function of ^{87}Rb atoms in an atomic lattice of strength V_0. Images were obtained after switching off the lattice potential suddenly and allowing atoms to expand for 15 ms. Potential strengths V_0 in units of the recoil energy E_R are a:0, b:3, c:7, d:10, e:13, f:14, g:16, and h:20 [202].

Fermionic atoms in optical lattices have also been studied. Köhl et al. [225] stored a large number of ^{40}K atoms in a three-dimensional simple cubic lattice and obtained absorption images after switching off the potential and allowing the atoms to expand ballistically. As the Pauli principle strictly forbids double occupation of single-particle energy levels, the fermionic ^{40}K atoms fill up the available Bloch states (11.6) up to the Fermi energy. The surface in $\vec{k}$ space which separates occupied states (at low energy) from empty states (at high energy) is called the Fermi surface. For a simple cubic optical lattice potential of the form (11.2) the Fermi surface is spherical at low density, but less so at higher density. For a completely filled band the Fermi surface is equal to the boundary of the first Brillouin zone. The energy gap to the next higher band then is the minimum energy for a single-particle excitation. For electrons in a solid that situation corresponds to an insulator (or a semiconductor, if the energy gap is small enough). In contrast to the interaction-induced Mott insulator discussed above, the present case is termed band insulator and obviously does not rely on interaction effects. In the optical-lattice experiment on ^{40}K the shape of the Fermi surface could be measured for various particle densities. Also, employing the magnetic-field dependence of the scattering between two spin species (Feshbach resonance), interaction effects like the transfer of atoms into higher bands could be observed.

These pioneering experiments on bosonic and fermionic atoms in optical lattices show that quantum simulation of correlated many-body systems may soon be within reach of experimental possibilities. These exciting prospects have led to a very large number of proposals for correlation effects in many-body systems that could be studied with atoms in optical lattices, see the review by Lewenstein et al. [218].

11.6.3 Universal optical lattice quantum computing?

The question mark in the title of this section implies the existence of problems impeding a straightforward implementation of quantum information processing in optical lattice systems. The most important of these problems is the lack of addressability of individual qubits. While the simulation of correlated quantum many-body systems profits from the fact that all atoms in an optical lattice are equal and in essentially the same environment, universal quantum computing suffers from this indistinguishability since the qubits cannot be addressed or manipulated individually, as necessary for running a non-trivial quantum algorithm.

To be able to distinguish between atoms the translational symmetry of the optical lattice must be broken. This can be achieved, for example, by applying a magnetic field gradient which makes the transition frequency of an atom depend on its position and

thus allows for different quantum operations at different positions. A more radical approach would be to abandon the three-dimensional optical lattice with its μm-size lattice constant and replace it with a two-dimensional array of focused laser beams with a single atom trapped in each laser focus [198, 199]. Each such focus is typically some μm in size and typical distances between neighboring foci are several tens of μm, so that individual atoms can be addressed with an additional focused laser beam. The necessary arrays of microlenses can be manufactured by microoptical techniques.

Review: quantum simulations with ultracold atomic gases [226]

Problems

For sufficiently large potential strength V_0 the optical lattice potential (11.2) can be approximated by a harmonic oscillator potential

$$V_{\text{osc}} = \frac{m\omega^2}{2}\vec{r}^2,$$

where $\vec{r}$ is the D-dimensional vector of displacement from the potential minimum.

a) Calculate the Hubbard interaction U (11.15), approximating the Wannier function $w_n(\vec{r})$ by the normalized oscillator ground-state wave function

$$\phi_0(\vec{r}) = \pi^{-D/4} a^{-D/2} \exp -\frac{1}{2}\left(\frac{\vec{r}}{a}\right)^2,$$

where $a = \sqrt{\frac{\hbar}{m\omega}}$ is the characteristic length of the quantum harmonic oscillator. Show that U grows as $V_0^{D/2}$.

b) The nearest-neighbor hopping amplitude t can be approximated by the overlap (the integral of the product of the wave functions) between the ground-state wave functions in neighboring potential wells. Calculate t and determine its dependence on the parameters of the optical lattice potential. Show that t decreases as V_0 grows.

11.5 Neutrale Atome und Quantencomputing/Quantensimulation

Gitter aus Licht

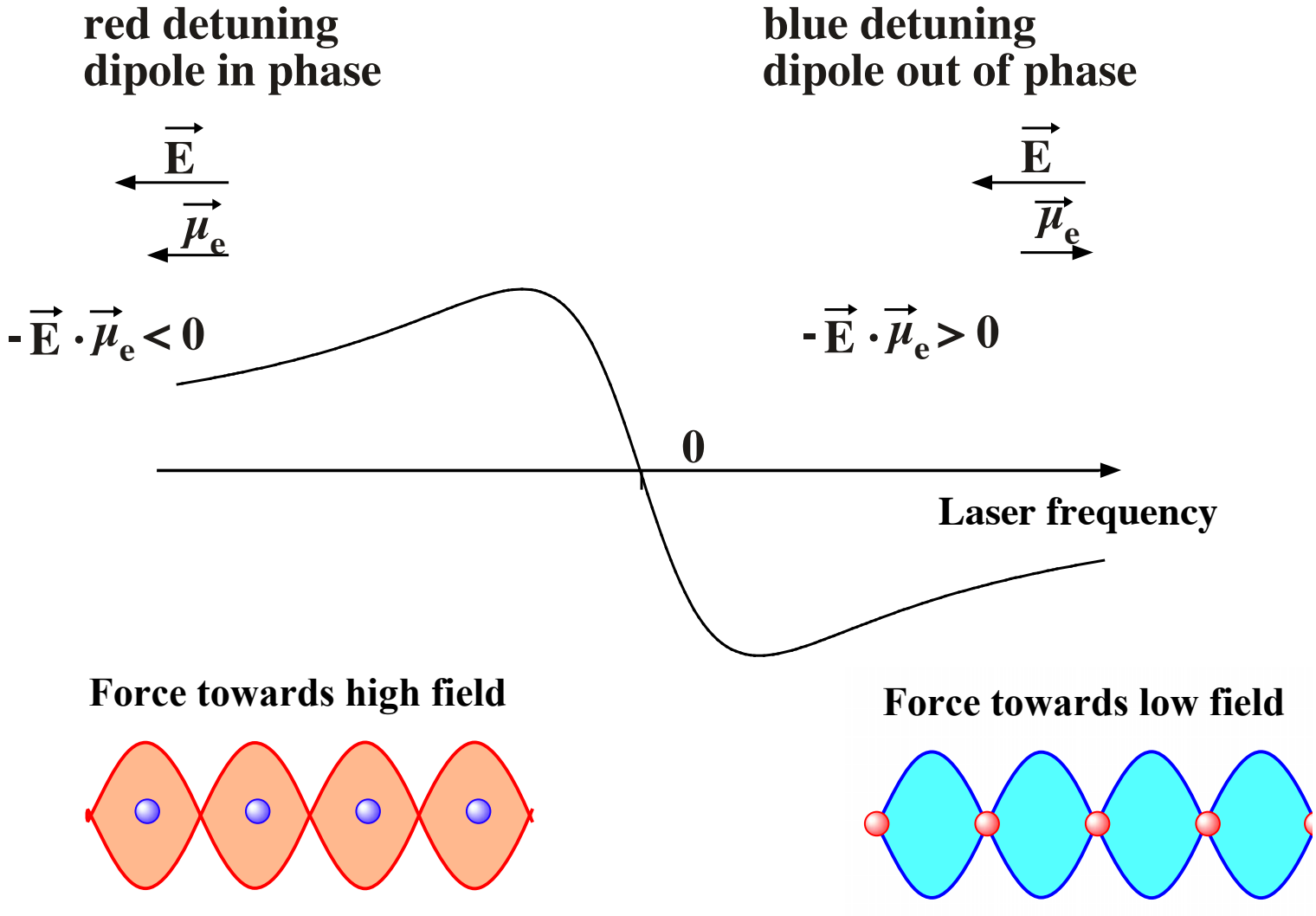

Eine stehende Laserwelle (Spiegel...) mit Frequenz oberhalb oder unterhalb einer Resonanz sorgt dafür, dass das Induzierte Dipolmoment der Atome gegenphasig oder gleichphasig mit dem Feld schwingt. Das elektrische Dipolmoment ist also entweder antiparallel zum Feld, so dass die Dipole (Atome) vom starken Feld abgestoßen werden, oder parallel zum Feld, so dass sie zum starken Feld hingezogen werden.

Gitter aus Linsen

Mit einer Matrix aus Mikrolinsen stellt man regelmäßig angeordnete Mikrobrennpunkte her, in denen sich Atome ansammeln.

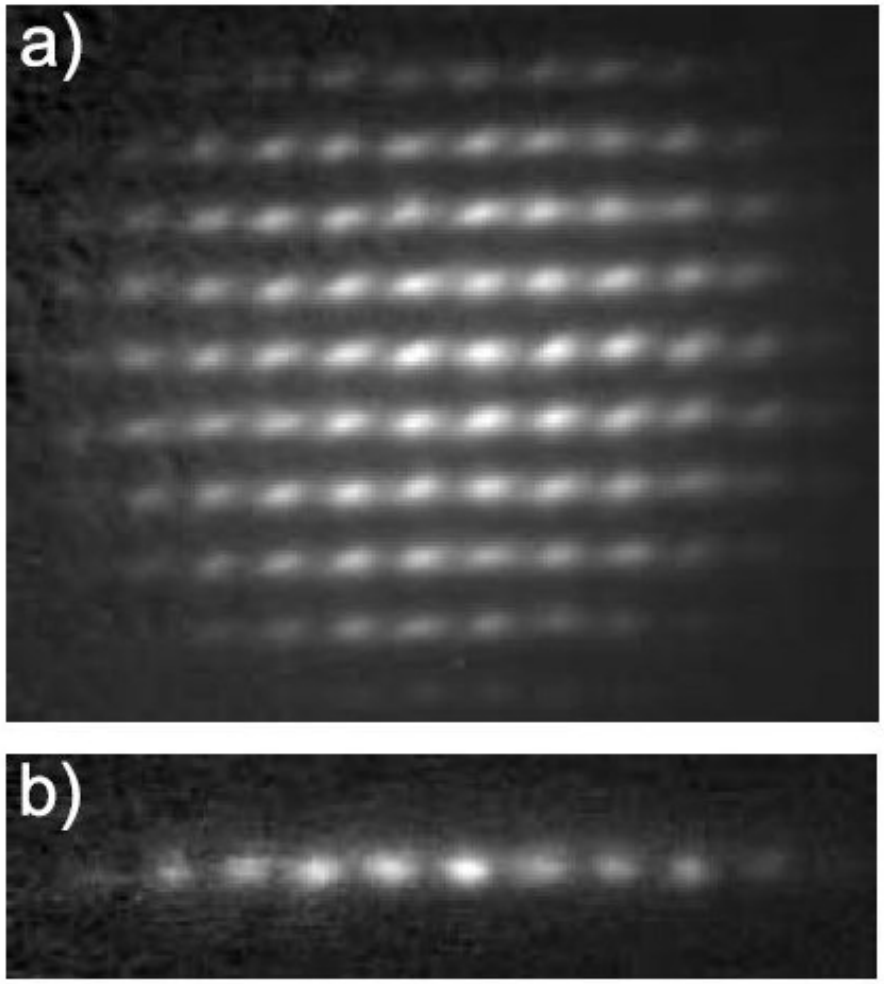

FIG. 1. (a) Two-dimensional and (b) one-dimensional arrays of rubidium atoms trapped in arrays of dipole traps. The traps are created using a micro-optical lens array and are separated by 125 μm. The brightest traps contain about 10^3 atoms.

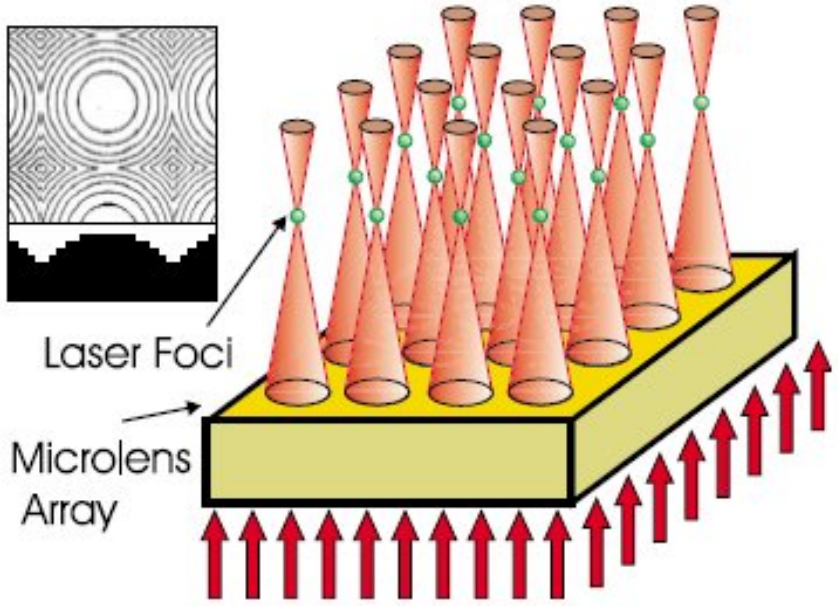

FIG. 2 (color online). A two-dimensional array of laser foci is created by focusing a single laser beam with an array of microlenses. Inset: Phase contrast image and typical cross section of a small part of a diffractive microlens array.

(Bilder aus Dumke et al. Phys. Rev. Lett. **89**, 097903 (2002))

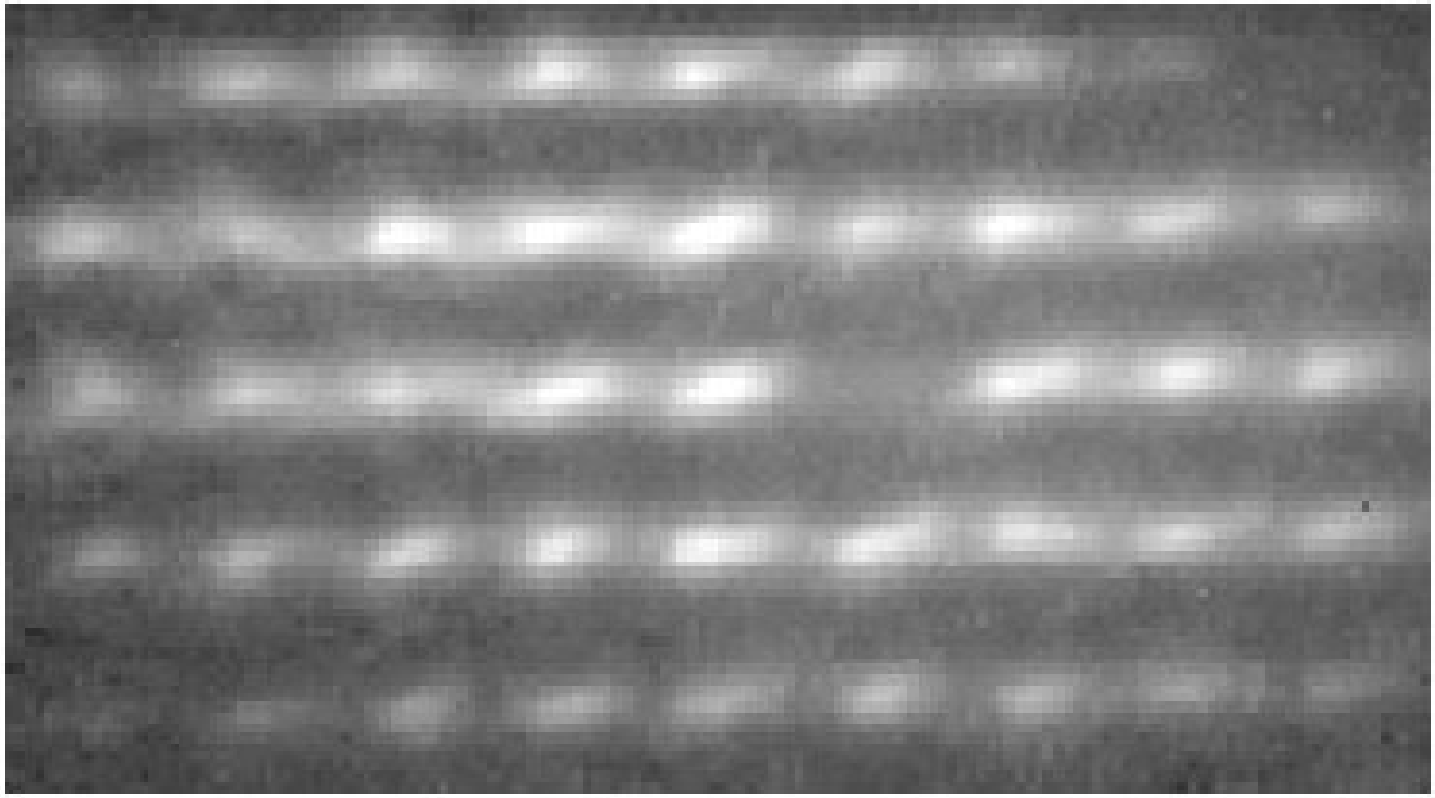

FIG. 3. Demonstration of the selective addressability of individual trap sites: By focusing a near-resonant laser beam onto one of the dipole traps (row 3, column 6) during the storage period, the atoms in this trap are removed, while the other dipole traps remain unaffected.

Atome sortieren mit Förderbändern aus Licht

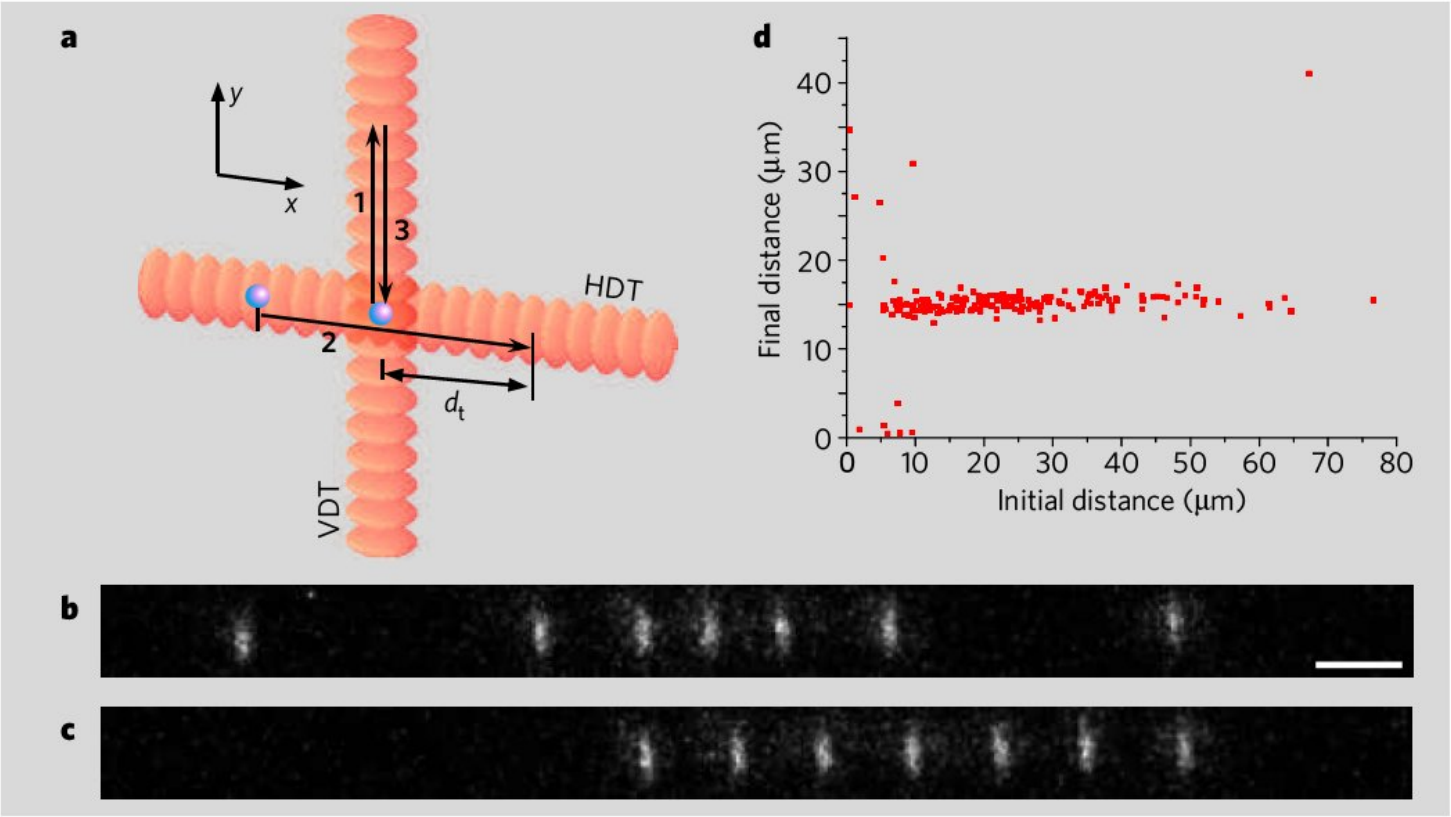

Figure 1 | Sorting atoms using optical tweezers. a, Two crossed standing-wave dipole traps are used to rearrange strings of trapped neutral atoms. (For methods, see supplementary information.) **b,** Fluorescence image of an initial string of seven randomly separated atoms. **c,** The same atoms after rearranging six of them using the distance-control operation. Scale bar, 15 μm. **d,** Relation between the final and the initial distance between simultaneously trapped atoms recorded for about 190 atom pairs. For initial distances greater than 10 μm, our distance-control operation successfully rearranges the atoms, resulting in a narrow distribution of final distances around the target distance $d_t = 15$ μm.

Langsame Phasenverschiebung (kleine Frequenzdifferenz) zwischen den gegenläufigen Strahlen bringt die stehende Welle zum Laufen $\longrightarrow$ „Förderband“.

Zwei zueinander senkrechte Förderbänder können benutzt werden, um Atome regelmäßig an gewünschten Stellen einzusortieren.

(Miroshnychenko et al., Nature **442**, 151 (2006); mit Videoclip)

11.6 Atome mit WW in optischen Gittern: Die etwas anderen Festkörper

NATURE | VOL 415 | 3 JANUARY 2002 | www.nature.com

Quantum phase transition from a superfluid to a Mott insulator in a gas of ultracold atoms

Markus Greiner*, Olaf Mandel*, Tilman Esslinger†, Theodor W. Hänsch* & Immanuel Bloch*

** Sektion Physik, Ludwig-Maximilians-Universität, Schellingstrasse 4/III, D-80799 Munich, Germany, and Max-Planck-Institut für Quantenoptik, D-85748 Garching, Germany*
† Quantenelektronik, ETH Zürich, 8093 Zurich, Switzerland

For a system at a temperature of absolute zero, all thermal fluctuations are frozen out, while quantum fluctuations prevail. These microscopic quantum fluctuations can induce a macroscopic phase transition in the ground state of a many-body system when the relative strength of two competing energy terms is varied across a critical value. Here we observe such a quantum phase transition in a Bose–Einstein condensate with repulsive interactions, held in a three-dimensional optical lattice potential. As the potential depth of the lattice is increased, a transition is observed from a superfluid to a Mott insulator phase. In the superfluid phase, each atom is spread out over the entire lattice, with long-range phase coherence. But in the insulating phase, exact numbers of atoms are localized at individual lattice sites, with no phase coherence across the lattice; this phase is characterized by a gap in the excitation spectrum. We can induce reversible changes between the two ground states of the system.

Feynmans Idee: Simuliere ein Quantensystem durch ein anderes!

Manipulationen mit Licht

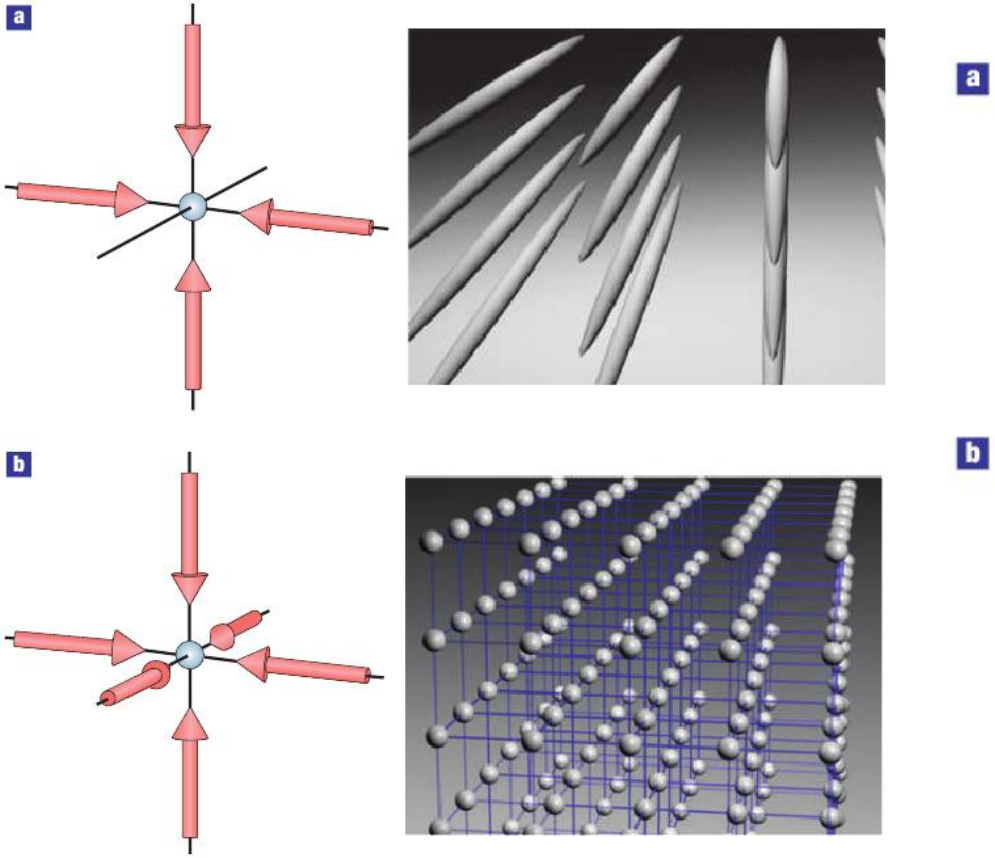

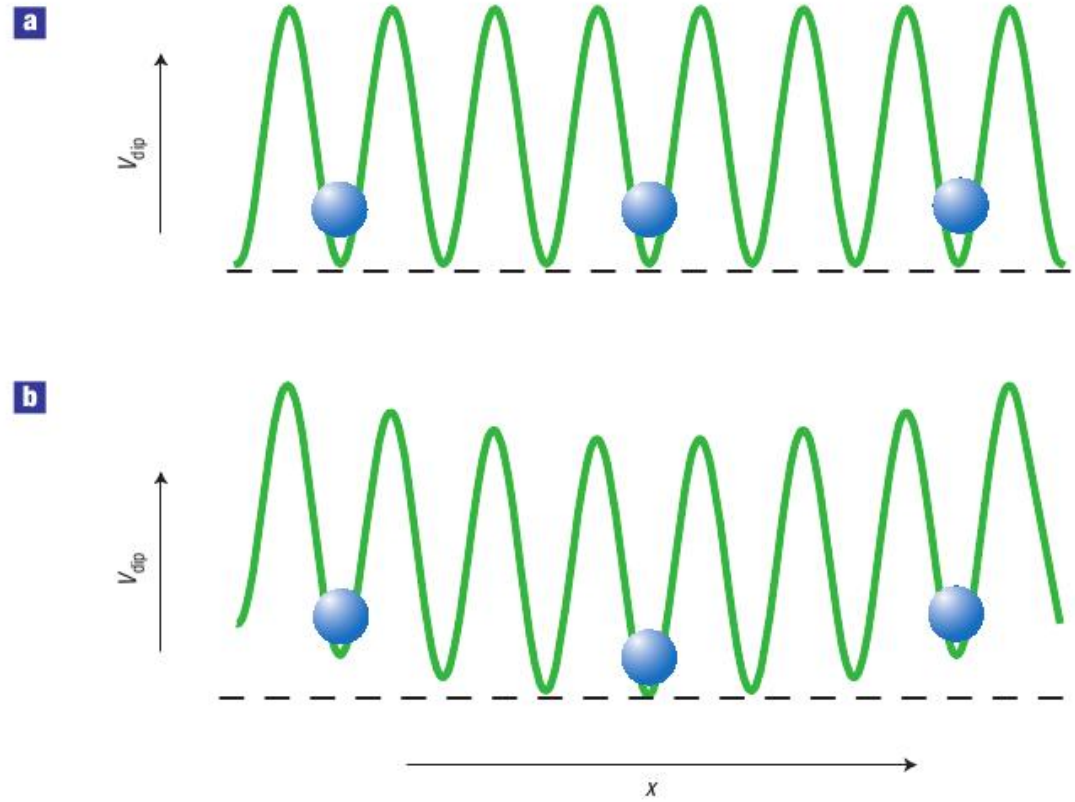

Aus Immanuel Bloch, Nature Physics **1**,23 (2005).

Verschiedene Phasen im Lichtkristall

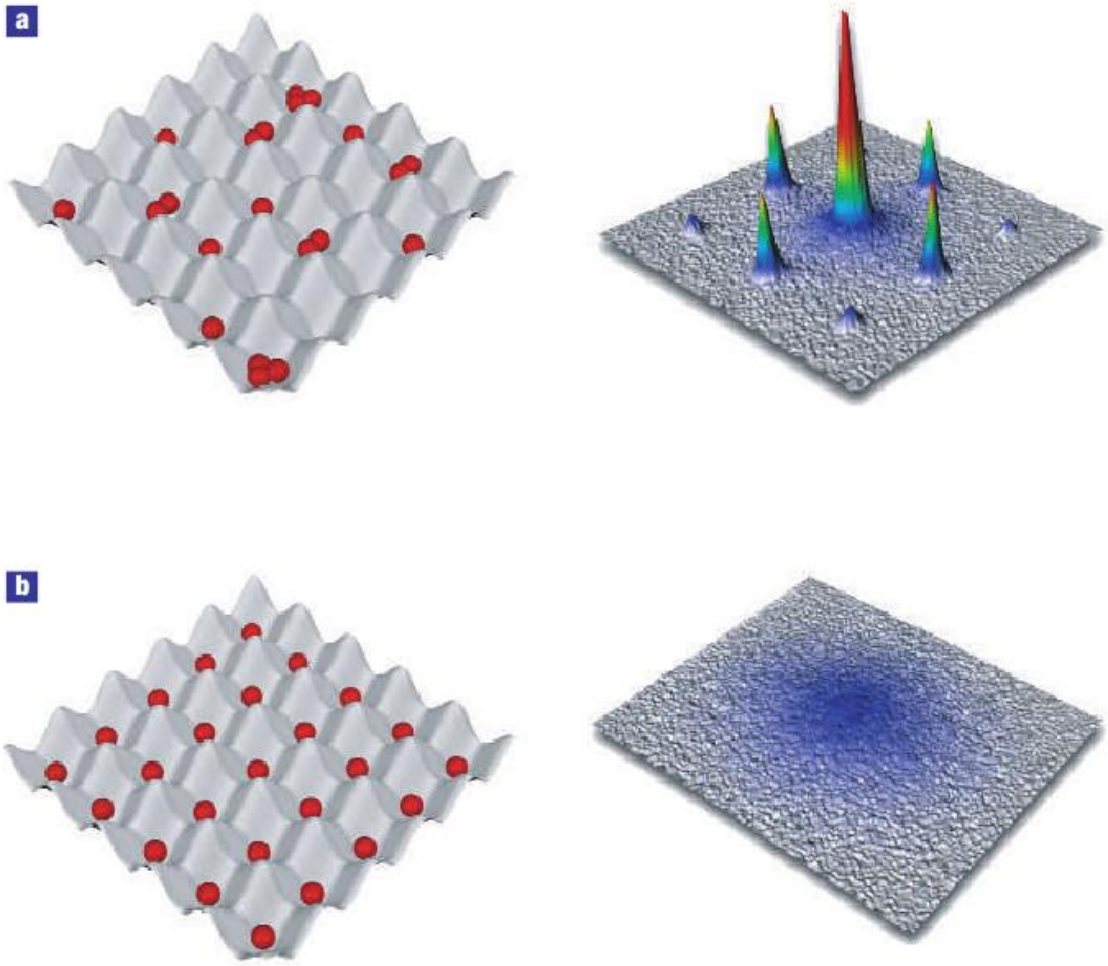

Links: Ortsraum; rechts: Impulsraum

Aus Immanuel Bloch, Nature Physics **1**,23 (2005).

Das Hubbard-Modell

Größenskalen:
„echter“ FK: $a \sim 10^{-10}$m, Elektron: punktförmig.
„Lichtkristall“: $a \sim \lambda_L \sim 10^{-6}$m, Atom: $r \sim a_B \sim 10^{-10}$m.

Potential des D-dimensionalen „Lichtkristalls“:

$$V(\vec{r}) = V_0 \sum_{i=1}^{D} \sin^2 k_L r_i$$

Überlagerung von D orthogonalen Laser-Stehwellen mit Wellenzahl $k_L = 2\pi/\lambda_L$. Potentialstärke $V_0 \sim$ Laserintensität; schwach $\vec{r}$-abhängig (Strahlprofil, Fokussierung)

Typische Energien

Wellenfunktion eines freien Teilchens:

$$\psi_{\vec{k}}(\vec{r}) = \frac{1}{\sqrt{\Omega}} e^{i\vec{k}\cdot\vec{r}}$$

(im Volumen Ω). Energie:

$$\varepsilon_{\vec{k}} = \frac{\hbar^2 k^2}{2m}.$$

Im Lichtgitter ist λ_L etwa gleich einer Resonanzwellenlänge. Wird ein λ_L-Photon absorbiert oder emittiert, gibt es eine Rückstoß-Energie

$$E_R = \frac{\hbar^2 k_L^2}{2m}.$$

Das ist die typische Energieskala.

Periodisches Potential: ebene Wellen werden gitterperiodisch moduliert $\rightarrow$ Blochfunktionen; Energiebänder weichen mehr oder weniger stark von Parabelform ab. Für schwaches Potential V_0 hat das niedrigste Band die maximale Energie (Rand der Brillouinzone)

$$\frac{\hbar^2}{2m}\left(\frac{\pi}{a}\right)^2 = \frac{\hbar^2}{2m}\left(\frac{2\pi}{\lambda_L}\right)^2 = \frac{\hbar^2 k_L^2}{2m} = E_R.$$

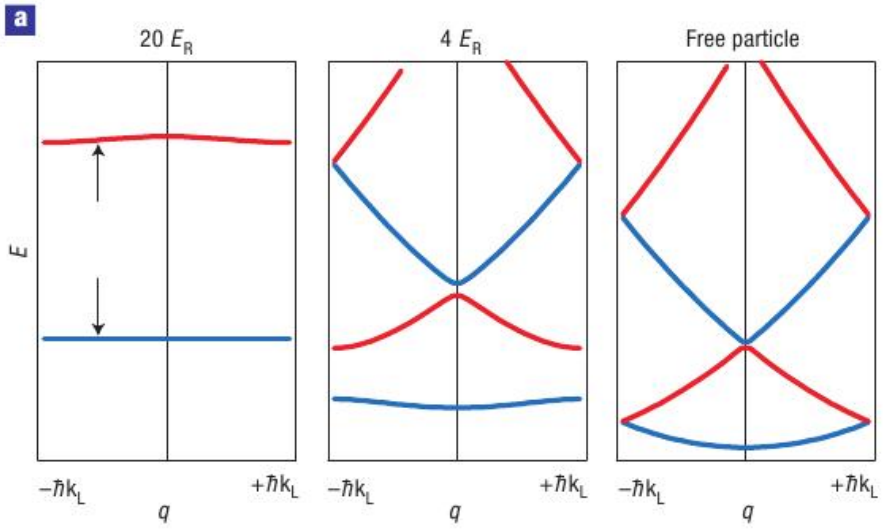

Bandstruktur für starkes (links), schwaches (Mitte) und verschwindendes Laser-Potential

Aus I. Bloch, Nature Physics **1**,23 (2005).

Hamiltonian nichtwechselwirkender Fermionen oder Bosonen in einem (z.B. optischen) Gitter

$$\mathbf{H} = \sum_{\vec{k},n} \varepsilon_{\vec{k},n} c^\dagger_{\vec{k},n} c_{\vec{k},n} \ ,$$

n ist der Bandindex; die Erzeuger und Vernichter beziehen sich auf Blochfunktionen; statdessen kann man (besser für unsere Diskussion) auch Wannierfunktionen nehmen.

$$w_n(\vec{r} - \vec{l}) = \frac{1}{\sqrt{N}} \sum_{\vec{k}} e^{-i\vec{k}\cdot\vec{l}} \psi_{n\vec{k}}(\vec{r}).$$

$\vec{l}$ ist der Gitterplatz, um den die Wannierfunktion zentriert ist. Für große Gitterabstände gehen die Wannierfunktionen in atomare Wellenfunktionen über. Hamiltonian, ausgedrückt im Wannierbild:

$$\mathbf{H} = \sum_{\vec{l},\vec{l}'} t_{\vec{l}-\vec{l}'n} c^{\dagger}_{\vec{l}n} c_{\vec{l}'n} \,,$$

wo die Hopping-Elemente $t_{\vec{l}-\vec{l}'n}$ angeben, mit welcher Wahrscheinlichkeitsamplitude ein Platzwechsel zwischen zwei Gitterplätzen stattfindet:

$$t_{\vec{l}-\vec{l}'n} = \frac{1}{N} \sum_{\vec{k}} \varepsilon_{\vec{k}n} e^{i\vec{k}\cdot(\vec{l}-\vec{l}')}.$$

Hopping-Elemente können auch als Überlapp-Matrixelemente zwischen Wannierfunktionen an den beiden beteiligten Gitterplätzen geschrieben werden.

Für starkes Potential V_0: Wannierfunktionen stark in ihrer jeweiligen Potentialmulde lokalisiert, Überlapp nur zwischen nächsten Nachbarn nennenswert $\longrightarrow$ nur ein Hopping-Element $-t_n$. Dann ist die Bandstruktur

$$\varepsilon_{\vec{k}n} = -2t_n \sum_{i=1}^{D} \cos k_i a.$$

$\vec{l}$ ist der Gitterplatz, um den die Wannierfunktion zentriert ist. Für große Gitterabstände gehen die Wannierfunktionen in atomare Wellenfunktionen über. Hamiltonian, ausgedrückt im Wannierbild:

$$\mathbf{H} = \sum_{\vec{l},\vec{l}'} t_{\vec{l}-\vec{l}'n} c^{\dagger}_{\vec{l}n} c_{\vec{l}'n} \,,$$

wo die Hopping-Elemente $t_{\vec{l}-\vec{l}'n}$ angeben, mit welcher Wahrscheinlichkeitsamplitude ein Platzwechsel zwischen zwei Gitterplätzen stattfindet:

$$t_{\vec{l}-\vec{l}'n} = \frac{1}{N} \sum_{\vec{k}} \varepsilon_{\vec{k}n} e^{i\vec{k}\cdot(\vec{l}-\vec{l}')}.$$

Hopping-Elemente können auch als Überlapp-Matrixelemente zwischen Wannierfunktionen an den beiden beteiligten Gitterplätzen geschrieben werden.

Für starkes Potential V_0: Wannierfunktionen stark in ihrer jeweiligen Potentialmulde lokalisiert, Überlapp nur zwischen nächsten Nachbarn nennenswert $\longrightarrow$ nur ein Hopping-Element $-t_n$. Dann ist die Bandstruktur

$$\varepsilon_{\vec{k}n} = -2t_n \sum_{i=1}^{D} \cos k_i a.$$

Und jetzt mit Wechselwirkung!

Welche Wechselwirkung? Wegen der Größenverhältnisse ist nur langreichweitiger Anteil interessant; parametrisierbar durch Streulänge a_S:

$$V_{\text{int}}(\vec{r}-\vec{r}') = \frac{4\pi\hbar^2}{m} a_S \delta(\vec{r}-\vec{r}').$$

Gestalt des Wechselwirkungs-Hamiltonians in Wannierdarstellung: Summe von Termen mit jeweils

- zwei Erzeugern und zwei Vernichtern
- einem Integral (Matrixelement) aus 4 Wannierfunktionen an 4 (oder weniger) Gitterplätzen und dem Wechselwirkungspotential.

Wegen starker Lokalisierung durch starkes Potential dominiert der Term, bei dem alle vier Wannierfunktionen an einem Platz sitzen. Die Wechselwirkung ist dann gegeben durch die Energie

$$U = \frac{4\pi\hbar^2}{m} a_S \int d^3r \, |w_n(\vec{r})|^4.$$

Wenn alles sich in einem Band abspielt, lassen wir den Bandindex n weg und erhalten für Spin-1/2-Fermionen das Hubbard-Modell:

$$\mathbf{H} = -t \sum_{\vec{l},\vec{l}',\sigma} c^{\dagger}_{\vec{l}\sigma} c_{\vec{l}'\sigma} + U \sum_{\vec{l}} n_{\vec{l}\uparrow} n_{\vec{l}\downarrow}$$

($\vec{l}, \vec{l}'$ nächste Nachbarn), $n_{\vec{l}\sigma} := c^{\dagger}_{\vec{l}\sigma} c_{\vec{l}\sigma}$ ist der Teilchenzahloperator. Das Pauliprinzip diktiert hier die Spin-Kombination im Wechselwirkungsterm: gleicher Spin ist verboten.

Bosonen mögen gleichen Spinzustand, und für Bosonen im gleichen Spinzustand ist das „Bose-Hubbard-Modell“

$$\mathbf{H} = -t \sum_{\vec{l},\vec{l}'} c^{\dagger}_{\vec{l}} c_{\vec{l}'} + \frac{U}{2} \sum_{\vec{l}} n_{\vec{l}}(n_{\vec{l}} - 1).$$

Wenn alles sich in einem Band abspielt, lassen wir den Bandindex n weg und erhalten für Spin-1/2-Fermionen das Hubbard-Modell:

$$\mathbf{H} = -t \sum_{\vec{l},\vec{l}',\sigma} c^\dagger_{\vec{l}\sigma} c_{\vec{l}'\sigma} + U \sum_{\vec{l}} n_{\vec{l}\uparrow} n_{\vec{l}\downarrow}$$

($\vec{l}, \vec{l}'$ nächste Nachbarn), $n_{\vec{l}\sigma} := c^\dagger_{\vec{l}\sigma} c_{\vec{l}\sigma}$ ist der Teilchenzahloperator. Das Pauliprinzip diktiert hier die Spin-Kombination im Wechselwirkungsterm: gleicher Spin ist verboten.

Bosonen mögen gleichen Spinzustand, und für Bosonen im gleichen Spinzustand ist das „Bose-Hubbard-Modell“

$$\mathbf{H} = -t \sum_{\vec{l},\vec{l}'} c^\dagger_{\vec{l}} c_{\vec{l}'} + \frac{U}{2} \sum_{\vec{l}} n_{\vec{l}}(n_{\vec{l}} - 1).$$

Der Steuerparameter des Hubbardmodells ist das Verhältnis t/U, und das kann mit dem Laser eingestellt werden:

$$U \sim V_0^{\frac{D}{4}} \qquad t \sim e^{-\text{const}\sqrt{V_0}}$$

Grenzfälle des Grundzustands sind gut verstanden.

Bose-Hubbard Hamiltonian for periodic lattice potential

$$H = -J\sum_{<i,j>}\hat{a}_i^{\dagger}\hat{a}_j + \sum_i \varepsilon_i \hat{n}_i + \frac{1}{2}U\sum_i \hat{n}_i(\hat{n}_i - 1)$$

Tunnel matrixelement J:

$$J = -\int d^3x\, w(\mathbf{x}-\mathbf{x}_i)\left(-\frac{\hbar^2}{2m}\nabla^2 + V_{lat}(\mathbf{x})\right)w(\mathbf{x}-\mathbf{x}_j)$$

On-site interaction energy U:

$$U = \frac{4\pi\hbar^2 a}{m}\int d^3x\,|w(\mathbf{x})|^4$$

$U/J < g_c$ ↓ two limits ↓ $U/J > g_c$

kinetic energy term dominates:

Weakly interacting bosonic gas

-> Superfluidity

- Atoms are **delocalized** over the entire lattice

$$|\Psi_{SF}\rangle \propto \left(\sum_{i=1}^{M}\hat{a}_i^{+}\right)^N |0\rangle$$

- Coherence, manybody state can be described by a **macroscopic wavefunction**

$$\langle a_i \rangle \neq 0$$

- **Coherent state**
  Superposition with a Binomial atom number distribution per lattice site
  -> number fluctuations

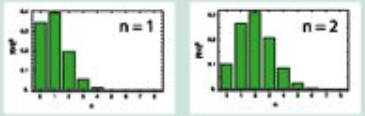

- **Gapless excitation spectrum**

interaction energy term dominates:

Strongly corrolated bosonic system

-> Mott insulator

- Atoms are completely **localized** to lattice sites

$$|\Psi_{Mott}\rangle \propto \prod_{i=1}^{M}\left(\hat{a}_i^{\dagger}\right)^n |0\rangle$$

- No coherence, no macroscopic wavefunction

$$\langle a_i \rangle = 0$$

- **Fock state**
  with a vanishing number fluctuation per lattice site

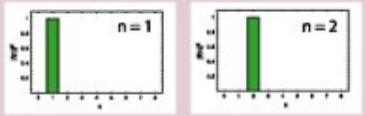

- **Excitation spectrum has an energy gap** $\Delta = U$

Vom k-Raum zum Ortsraum: Einfach abwarten...

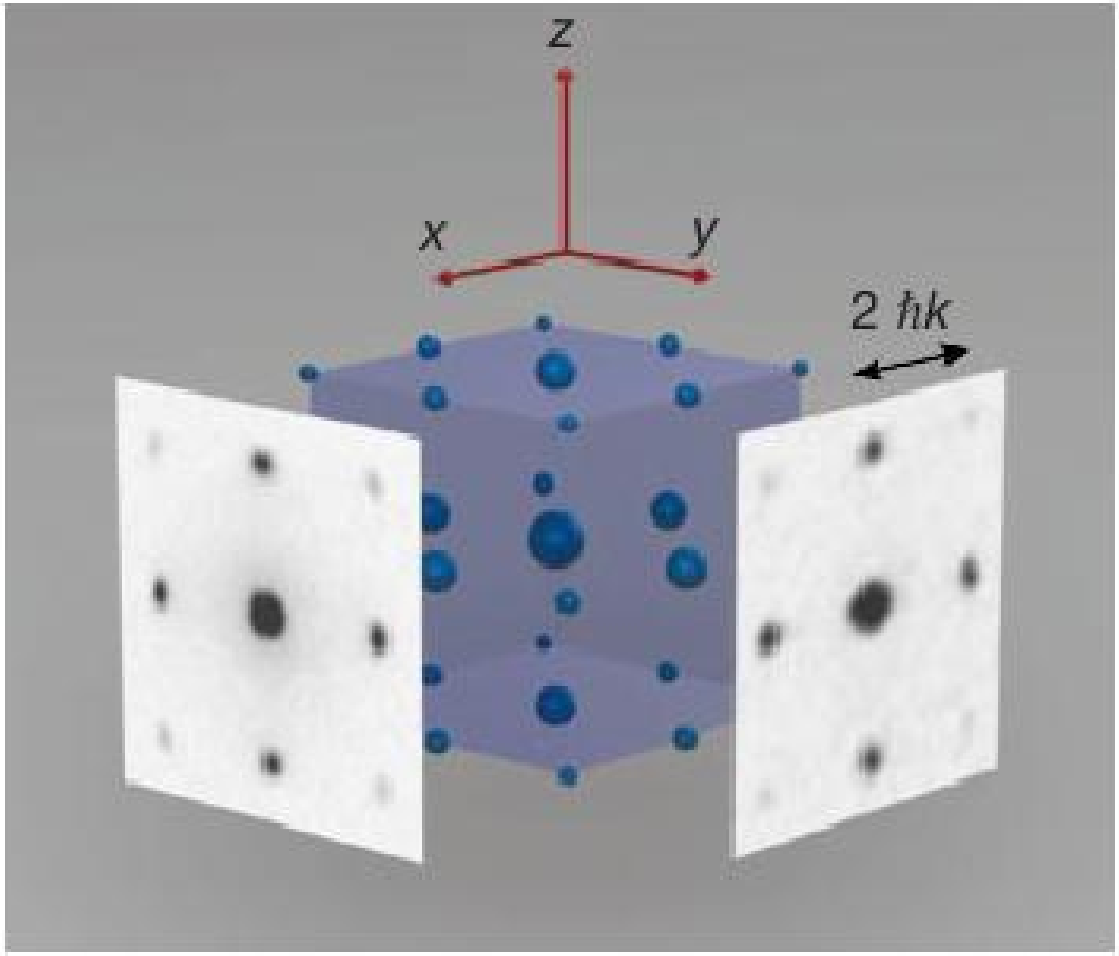

Figure 1 Schematic three-dimensional interference pattern with measured absorption images taken along two orthogonal directions. The absorption images were obtained after ballistic expansion from a lattice with a potential depth of $V_0 = 10E_r$ and a time of flight of 15 ms.

^{87}Rb

Aus Greiner et al. Nature **415**, 39 (2002)

Der Mott-Hubbard-Übergang: Live und in Farbe

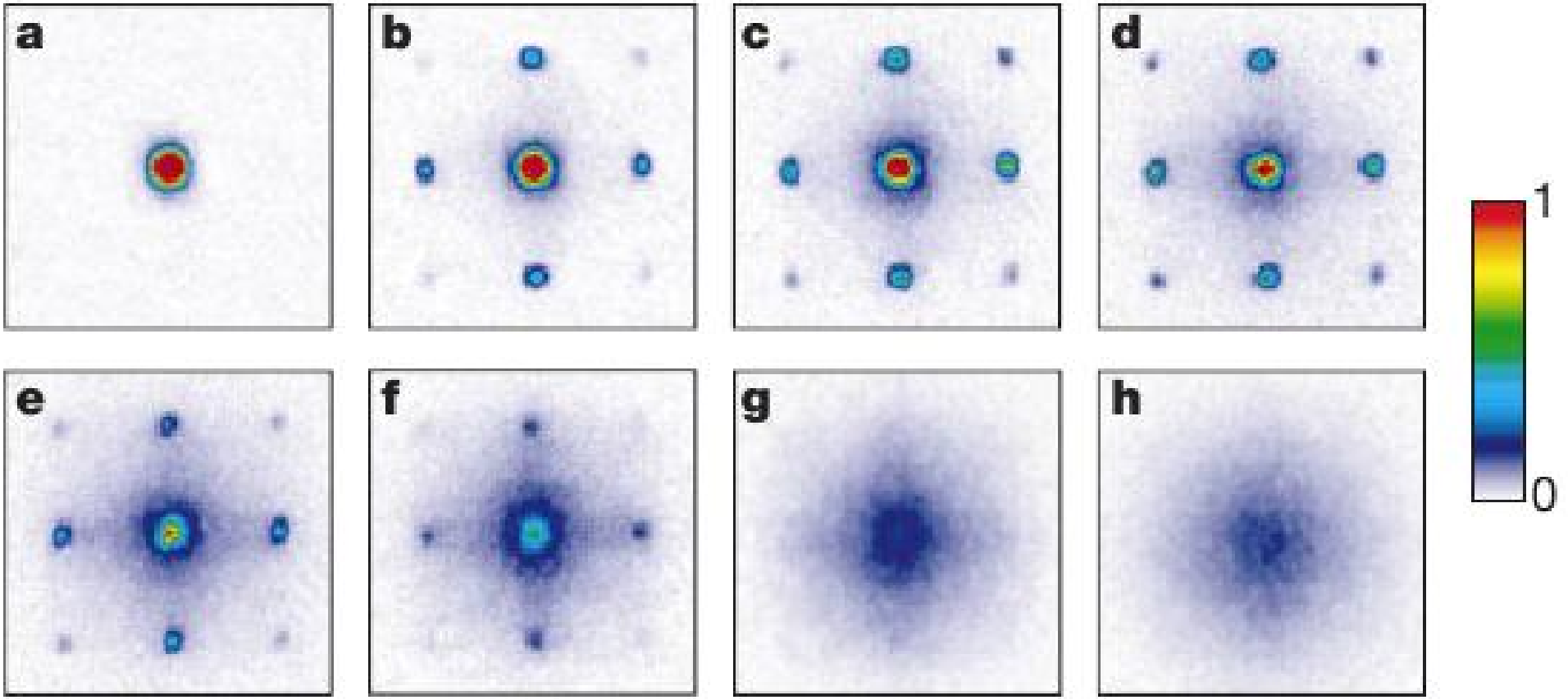

Figure 2 Absorption images of multiple matter wave interference patterns. These were obtained after suddenly releasing the atoms from an optical lattice potential with different potential depths V_0 after a time of flight of 15 ms. Values of V_0 were: **a**, 0 E_r; **b**, 3 E_r; **c**, 7 E_r; **d**, 10 E_r; **e**, 13 E_r; **f**, 14 E_r; **g**, 16 E_r; and **h**, 20 E_r.

Aus Greiner et al. Nature **415**, 39 (2002)

Kollaps und Wiederbelebung

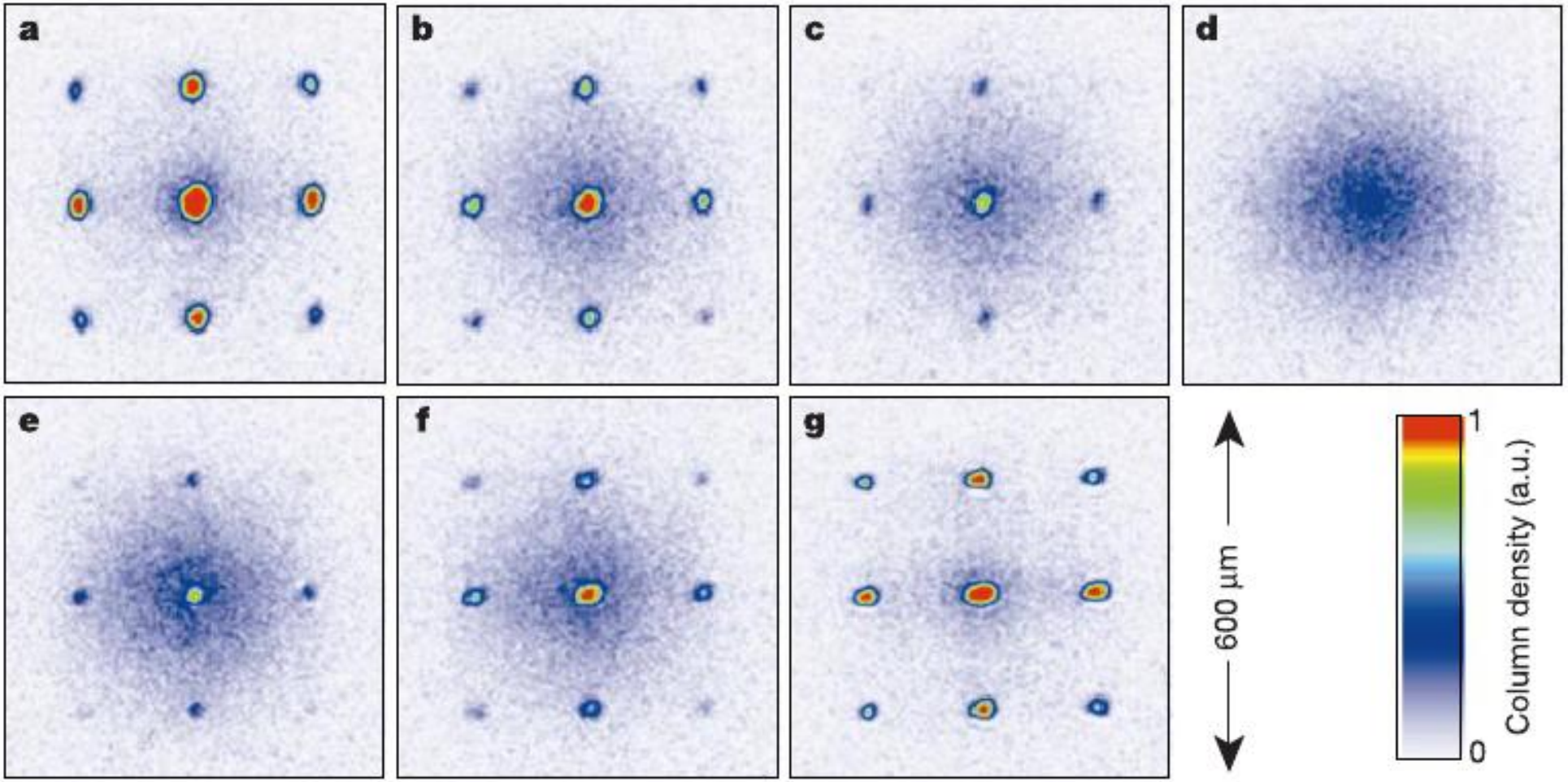

Aus Greiner et al. Nature **419**, 51 (2002)

Plötzliches Umschalten von t/U macht aus einem Eigenzustand des Hamiltonians eine Superposition, die Oszillationen zeigt.

Fermisystem ohne Wechselwirkung : Fermifläche

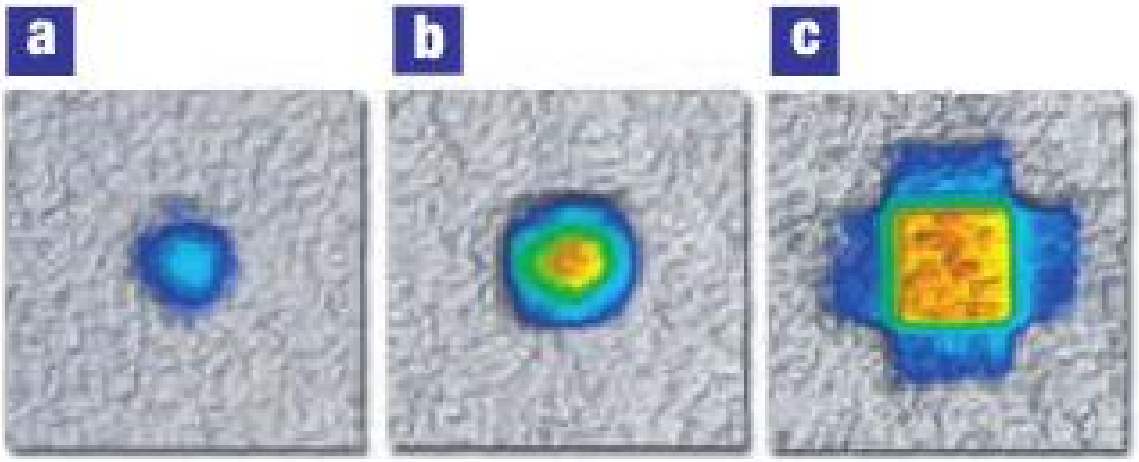

Figure 7 Observing Fermi surfaces. **a–c**, Time-of-flight images of an ultracold Fermi gas of ^{40}K atoms released from a 3D optical lattice potential for increasing filling factors corresponding to different Fermi energies. An adiabatic ramp-down of the lattice potential maps the crystal momentum of the particles onto free particle momentum, such that the band population can be directly observed in the time of flight absorption images (with kind permission from T. Esslinger, ETH Zurich, see also ref. 24).

Aus Immanuel Bloch, Nature Physics **1**,23 (2005).

Fermisystem mit Wechselwirkung

Metallic and Insulating Phases of Repulsively Interacting Fermions in a 3D Optical Lattice

U. Schneider,[1] L. Hackermüller,[1] S. Will,[1] Th. Best,[1] I. Bloch,[1,2]* T. A. Costi,[3] R. W. Helmes,[4] D. Rasch,[4] A. Rosch[4]

The fermionic Hubbard model plays a fundamental role in the description of strongly correlated materials. We have realized this Hamiltonian in a repulsively interacting spin mixture of ultracold ^{40}K atoms in a three-dimensional (3D) optical lattice. Using in situ imaging and independent control of external confinement and lattice depth, we were able to directly measure the compressibility of the quantum gas in the trap. Together with a comparison to ab initio dynamical mean field theory calculations, we show how the system evolves for increasing confinement from a compressible dilute metal over a strongly interacting Fermi liquid into a band-insulating state. For strong interactions, we find evidence for an emergent incompressible Mott insulating phase. This demonstrates the potential to model interacting condensed-matter systems using ultracold fermionic atoms.

Sauberer Festkörper ohne Fehlstellen, Gitterschwingungen...; mit kontrollierbaren Parametern:

$2 \cdot 10^5$ ^{40}K-Atome in den Gesamtspinzuständen $|F, m_F\rangle = |\frac{9}{2}, -\frac{9}{2}\rangle = |\downarrow\rangle$ und $|\frac{9}{2}, -\frac{7}{2}\rangle = |\uparrow\rangle$ ...

...in einem (Licht-) Potential aus zwei unabhängigen Komponenten: periodisch + parabolisch.

Parabolisches Potential drückt die Fermionen im (festen) Gitter zusammen; im realen Festkörper wird das Gitter bei Kompressibilitätsmessungen dagegen immer mit komprimiert.

Hubbardmodell:

$$\mathbf{H} = -t \sum_{\vec{l},\vec{l}',\sigma} c^\dagger_{\vec{l}\sigma} c_{\vec{l}'\sigma} + U \sum_{\vec{l}} n_{\vec{l}\uparrow} n_{\vec{l}\downarrow} + \sum_{\vec{l}} V_{\text{Parabel}}(\vec{l})(n_{\vec{l}\uparrow} + n_{\vec{l}\downarrow})$$

Das Hubbard-U kann über eine Feshbach-Resonanz gesteuert werden (Streulänge; vgl. Duine und Stoof, Physics Reports **396**, 115 (2004)).

Achtung: t heißt bei den Atomphysikern immer J.

Sauberer Festkörper ohne Fehlstellen, Gitterschwingungen...; mit kontrollierbaren Parametern:

$2 \cdot 10^5$ ^{40}K-Atome in den Gesamtspinzuständen $|F, m_F\rangle = |\frac{9}{2}, -\frac{9}{2}\rangle = |\downarrow\rangle$ und $|\frac{9}{2}, -\frac{7}{2}\rangle = |\uparrow\rangle$ ...

...in einem (Licht-) Potential aus zwei unabhängigen Komponenten: periodisch + parabolisch.

Parabolisches Potential drückt die Fermionen im (festen) Gitter zusammen; im realen Festkörper wird das Gitter bei Kompressibilitätsmessungen dagegen immer mit komprimiert.

Hubbardmodell:

$$\mathbf{H} = -t \sum_{\vec{l},\vec{l}',\sigma} c^\dagger_{\vec{l}\sigma} c_{\vec{l}'\sigma} + U \sum_{\vec{l}} n_{\vec{l}\uparrow} n_{\vec{l}\downarrow} + \sum_{\vec{l}} V_{\text{Parabel}}(\vec{l})(n_{\vec{l}\uparrow} + n_{\vec{l}\downarrow})$$

Das Hubbard-U kann über eine Feshbach-Resonanz gesteuert werden (Streulänge; vgl. Duine und Stoof, Physics Reports **396**, 115 (2004)).

Achtung: t heißt bei den Atomphysikern immer J.

Was erwartet man?

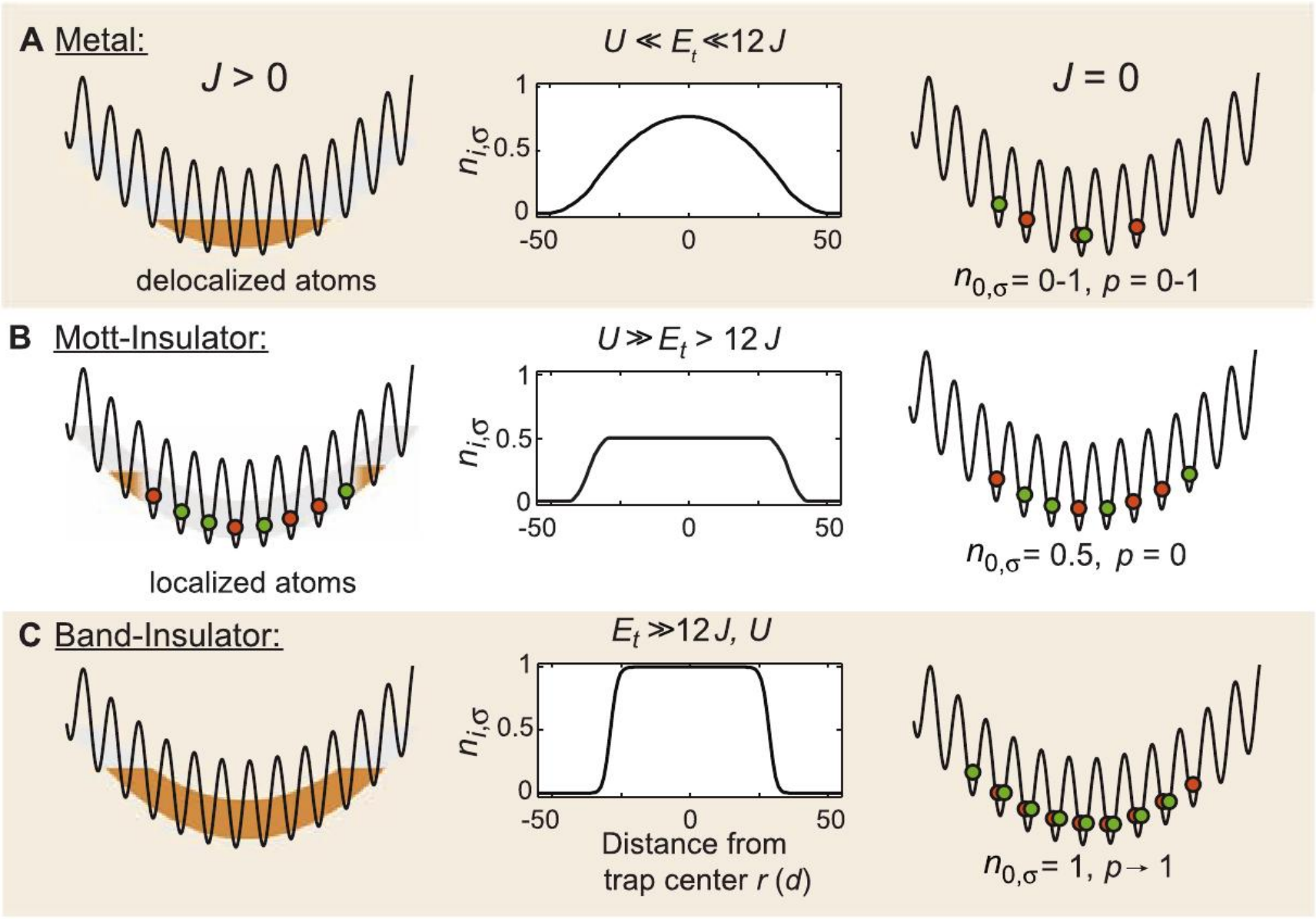

Isolator-Phasen sind inkompressibel: Doppelbesetzung oder Transfer in höheres Energieband sind teuer.

Fig. 1. (**A** to **C**) Relevant phases of the Hubbard model with an inhomogeneous trapping potential for a spin mixture at $T = 0$. A schematic is shown in the left column. The center column displays the corresponding in-trap density profiles, and the right column outlines the distribution of singly and doubly occupied lattice sites after a rapid projection into the zero tunneling limit, with p denoting the total fraction of atoms on doubly occupied lattice sites.

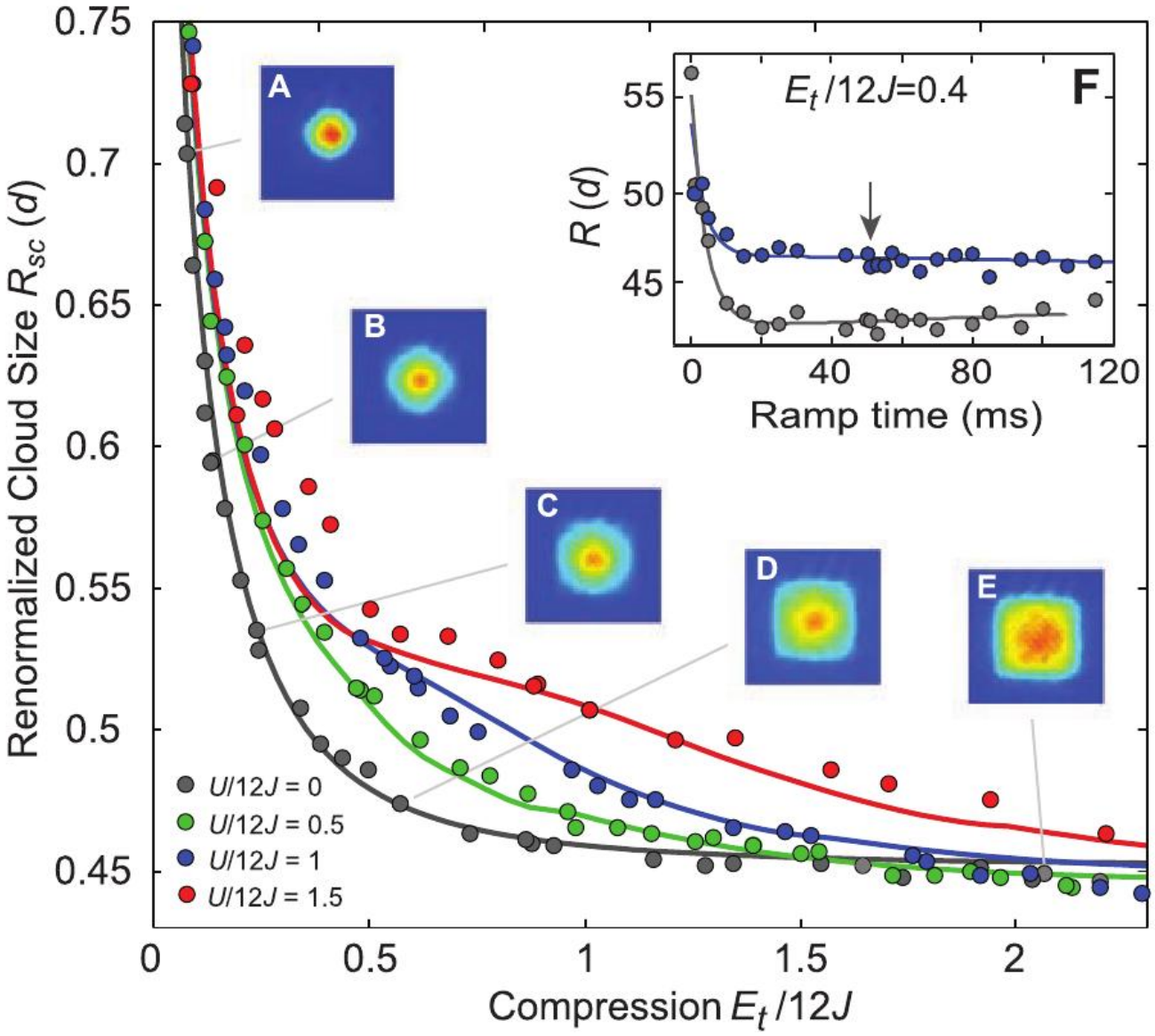

Fig. 3. Cloud sizes of the interacting spin mixture versus compression. Measured cloud size R_{sc} in a $V_{lat} = 8\ E_r$ deep lattice as a function of the external trapping potential for various interactions $U/12J$ = 0...1.5 is shown. Dots denote single experimental shots, lines denote the theoretical expectation from DMFT for an initial temperature $T/T_F = 0.15$. The insets **(A** to **E)** show the quasi-momentum distribution of the noninteracting clouds (averaged over several shots). **(F)** Resulting cloud size for different lattice ramp times at $E_t/12J$ = 0.4 for a noninteracting and an interacting Fermi gas. The arrow marks the ramp time of 50 ms used in the experiment.

Größe der Atomwolke in Abhängigkeit von der Kompressionsstärke, für verschiedene Werte der Hubbard-Abstoßung U.

Bilder zeigen die Fermifläche (für $U = 0$); bei E ist das Band voll; weitere Kompression unmöglich.

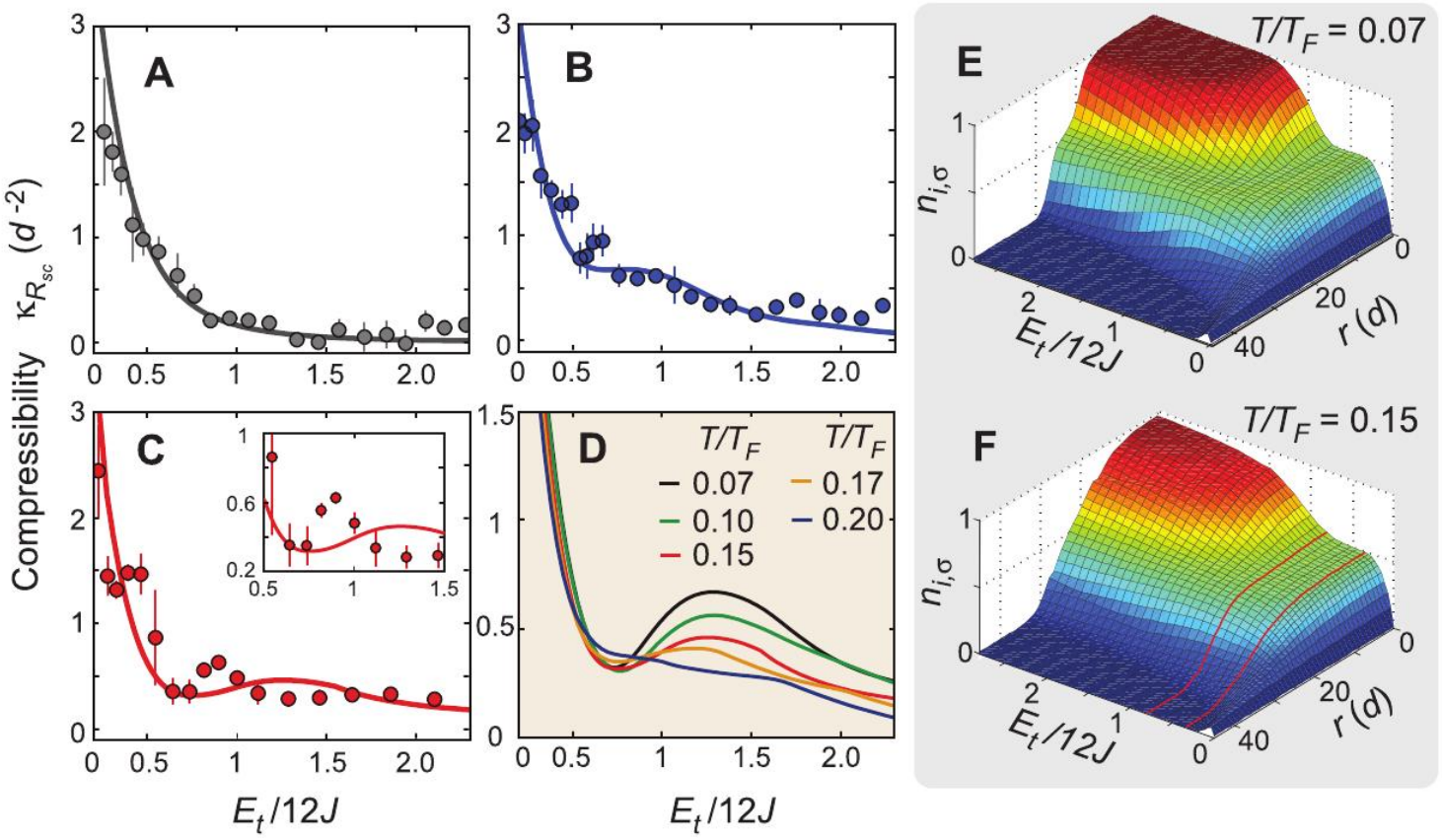

Fig. 4. Compressibility and in-trap density distribution. (**A** to **C**) Global compressibility $\kappa_{R_{sc}}$ of the atom cloud for various interactions [(A) $U/12J = 0$, (B) $U/12J = 1$, (C) $U/12J = 1.5$]. Dots denote the result of linear fits on the measured data, and the error bars represent the fit uncertainty. Solid lines display the theoretically expected results for an initial temperature $T/T_F = 0.15$. The influence of the initial temperature on the calculated compressibility is shown in (**D**) for $U/12J = 1.5$. The corresponding density distributions are plotted in (**E**) and (**F**), with r denoting the distance to the trap center (see also figs. S7 and S8). The red lines mark the region where a Mott insulating core has formed and the global compressibility is reduced.

Rechte Seite: „Hochzeitstorten“-Struktur der Dichte, mit Plateaus bei einem (Mott-Isolator) bzw zwei (alles voll) Teilchen pro Gitterplatz.
(Beachte: Hier ist die Zahl der Teilchen pro Platz und Spinrichtung aufgetragen → Faktor 2.)

Kompressibilität in Abhängigkeit von der Kompressionsstärke, für verschiedene Werte der Hubbard-Abstoßung U. Das Minimum in der Kurve C ist die Signatur des Mott-Isolators (1 Fermion pro Gitterplatz).

Noch ein Trick: Künstliche Magnetfelder

Neutrale Atome können an reale Magnetfelder höchstens schwach über ihre Dipolmomente koppeln $\rightarrow$ Studium der Effekte von Magnetfeldern auf geladene Teilchen (Quanten-Hall-Effekt...) ist in diesen Modellsystemen nicht möglich.

Noch ein Trick: Künstliche Magnetfelder

Neutrale Atome können an reale Magnetfelder höchstens schwach über ihre Dipolmomente koppeln $\rightarrow$ Studium der Effekte von Magnetfeldern auf geladene Teilchen (Quanten-Hall-Effekt...) ist in diesen Modellsystemen nicht möglich.

Oder vielleicht doch?

Noch ein Trick: Künstliche Magnetfelder

Neutrale Atome können an reale Magnetfelder höchstens schwach über ihre Dipolmomente koppeln $\rightarrow$ Studium der Effekte von Magnetfeldern auf geladene Teilchen (Quanten-Hall-Effekt...) ist in diesen Modellsystemen nicht möglich.

Oder vielleicht doch?

Wie wirkt ein Magnetfeld auf ein geladenes Teilchen?

$$\vec{p} \longrightarrow \vec{p} - q\vec{A}(\vec{r})$$

bewirkt eine zusätzliche ortsabhängige Phasenverschiebung in der Wellenfunktion.

Noch ein Trick: Künstliche Magnetfelder

Neutrale Atome können an reale Magnetfelder höchstens schwach über ihre Dipolmomente koppeln → Studium der Effekte von Magnetfeldern auf geladene Teilchen (Quanten-Hall-Effekt...) ist in diesen Modellsystemen nicht möglich.

Oder vielleicht doch?

Wie wirkt ein Magnetfeld auf ein geladenes Teilchen?

$$\vec{p} \longrightarrow \vec{p} - q\vec{A}(\vec{r})$$

bewirkt eine zusätzliche ortsabhängige Phasenverschiebung in der Wellenfunktion.

Versuche eine derartige Phasenverschiebung auf optischem Weg zu erreichen.

nature Vol 462|3 December 2009|doi:10.1038/nature08609

LETTERS

Synthetic magnetic fields for ultracold neutral atoms

Y.-J. Lin[1], R. L. Compton[1], K. Jiménez-García[1,2], J. V. Porto[1] & I. B. Spielman[1]

Bose-Einstein-Kondensat aus bis zu 2.5 $\cdot 10^5$ ^{87}Rb-Atomen.
Der Grundzustand hat Gesamtspin $F = 1$.
$m_F = 0, \pm 1$ spalten in einem Magnetfeld auf. Die Atome bewegen sich gemäß der Dispersionsrelation

$$E(\vec{k}, m_F) = \frac{\hbar^2 k^2}{2m} + \hbar \omega_Z m_F$$

(ω_Z = Zeeman-Aufspaltung).

Raman-Prozess koppelt die verschiedenen m_F-Komponenten aneinander: Emission und Absorption von zwei Photonen mit passender Differenzfrequenz, nahe dem Übergang zu einem angeregten Hilfszustand.

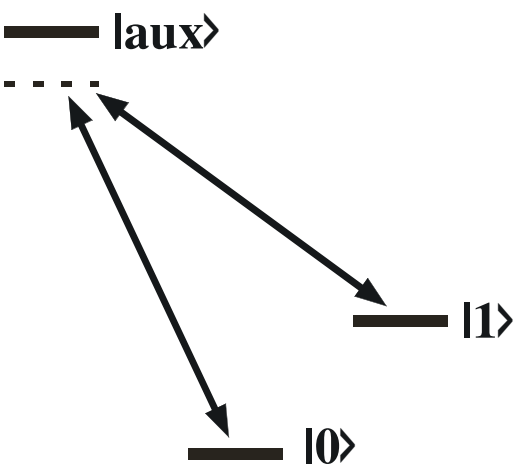

Trick: Verwende zwei Raman-Laser unterschiedlicher Strahlrichtung
$\rightarrow$ m_F-abhängiger Impulsübertrag auf das Atom.

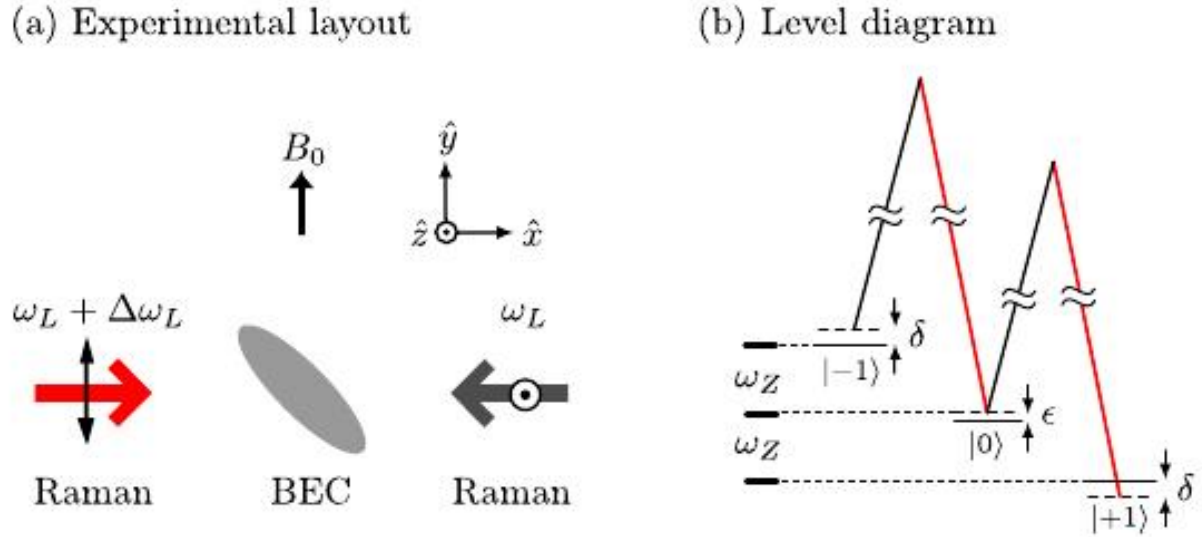

(Aus Lin et al. Phys. Rev. Lett. **102**, 130401 (2009))

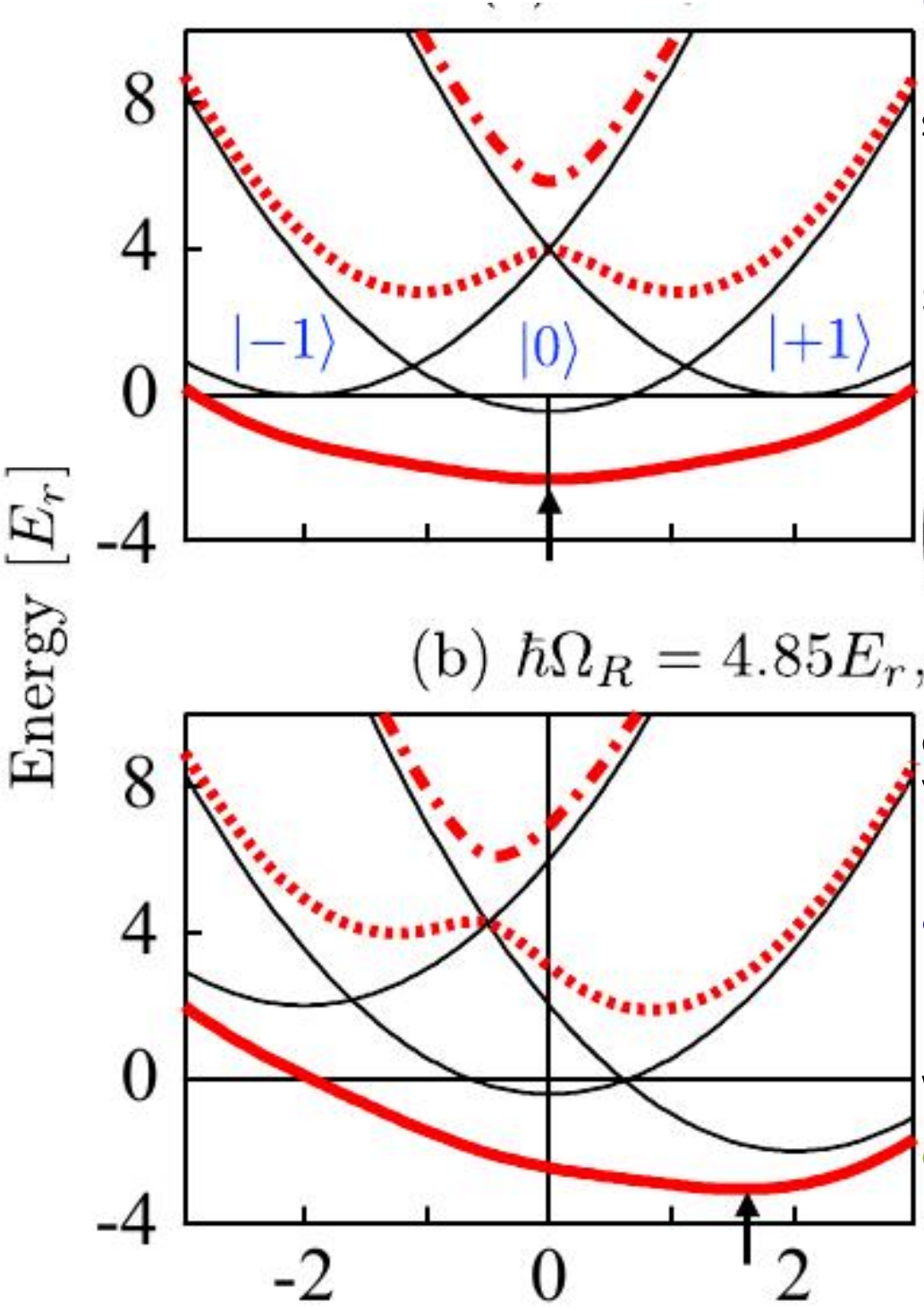

Oberes Bild:

Die Parabel-Dispersionen der Atome mit unterschiedlichem m_F sind gegeneinander verschoben (dünne schwarze Linien). Der Raman-Prozess koppelt die Zustände mit einer Stärke (Rabifrequenz) Ω_R. In der Rotating-Wave-Approximation hat die Hamiltonmatrix für den relevanten Unterraum die Gestalt:

$$\begin{pmatrix} \frac{\hbar}{2m}(\tilde{k}_x + 2k_r)^2 - \delta & \Omega_R/2 & 0 \\ \Omega_R/2 & \frac{\hbar}{2m}\tilde{k}_x^2 - \epsilon & \Omega_R/2 \\ 0 & \Omega_R/2 & \frac{\hbar}{2m}(\tilde{k}_x - 2k_r)^2 + \delta \end{pmatrix}$$

(δ: Verstimmung der Ramanlaser-Frequenzdifferenz gegenüber ω_Z, ϵ ist die Zeeman-Verschiebung 2. Ordnung für $m_F = 0$.) Die Eigenwerte sind die **dicken roten** Linien, für $\delta = 0$. Das Minimum liegt bei $k = 0$.

Unteres Bild:

Wie oben, aber $\delta \neq 0$; das Minimum liegt bei einem endlichen k:

$$E(k) - E_0 \approx \frac{1}{2m}(\hbar(k - k_0))^2 = \frac{1}{2m}(p - \tilde{q}\tilde{A})^2$$

Das synthetische Vektorpotential $\tilde{A}$ hängt von der Verstimmung δ ab, die über das (reale) Magnetfeld ortsabhängig gemacht werden kann $\rightarrow$ synthetisches Magnetfeld.

Das Bose-Einstein-Kondensat besitzt eine gemeinsame makroskopische Wellenfunktion $\rightarrow$ Flussquantisierung des (synth.) Magnetfelds, ähnlich wie beim Supraleiter. Flussquanten äußern sich als Wirbellinien (vortices).

Diese wurden (mit einer etwas anderen Geometrie als oben beschrieben) von Lin et al. (Nature **462**, 628 (2009)) beobachtet.

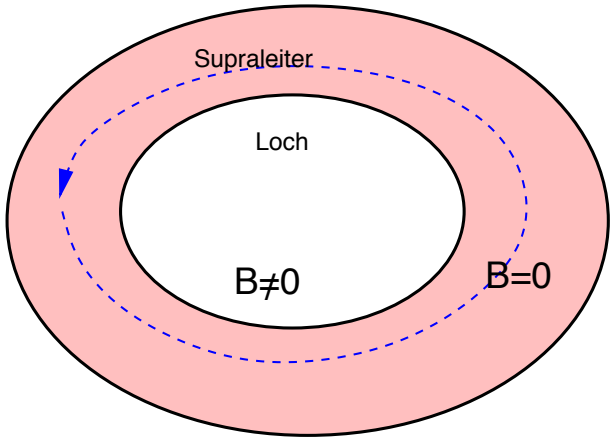

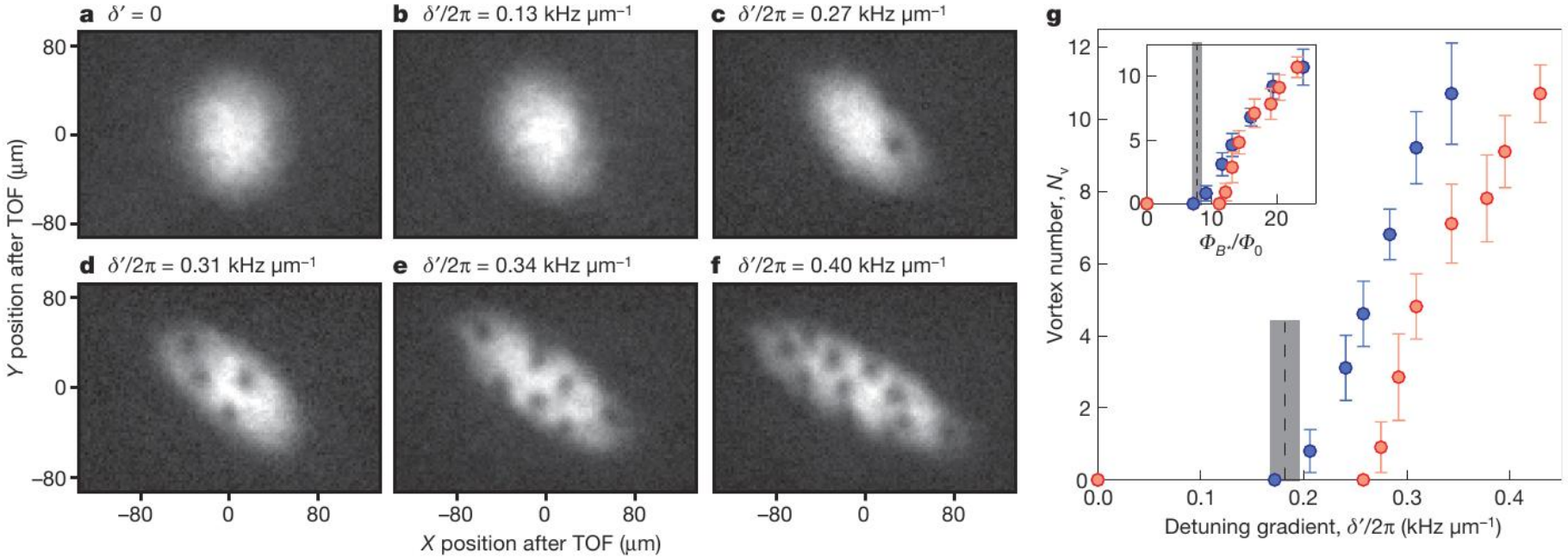

Figure 2 | Appearance of vortices at different detuning gradients. Data was taken for $N = 1.4 \times 10^5$ atoms at hold time $t_h = 0.57$ s. **a–f**, Images of the $|m_F = 0\rangle$ component of the dressed state after a 25.1-ms TOF with detuning gradient $\delta'/2\pi$ from 0 to 0.43 kHz μm^{-1} at Raman coupling $\hbar\Omega_R = 8.20E_L$. **g**, Vortex number N_v versus δ' at $\hbar\Omega_R = 5.85E_L$ (blue circles) and $8.20E_L$ (red circles). Each data point is averaged over at least 20 experimental realizations, and the uncertainties represent one standard deviation σ. The inset displays N_v versus the synthetic magnetic flux $\Phi_{B^*}/\Phi_0 = \mathcal{A}q^*\langle B^*\rangle/h$ in the BEC. The dashed lines indicate δ', below which vortices become energetically unfavourable according to our GPE computation, and the shaded regions show the 1σ uncertainty from experimental parameters.

Einige experimentelle Details:

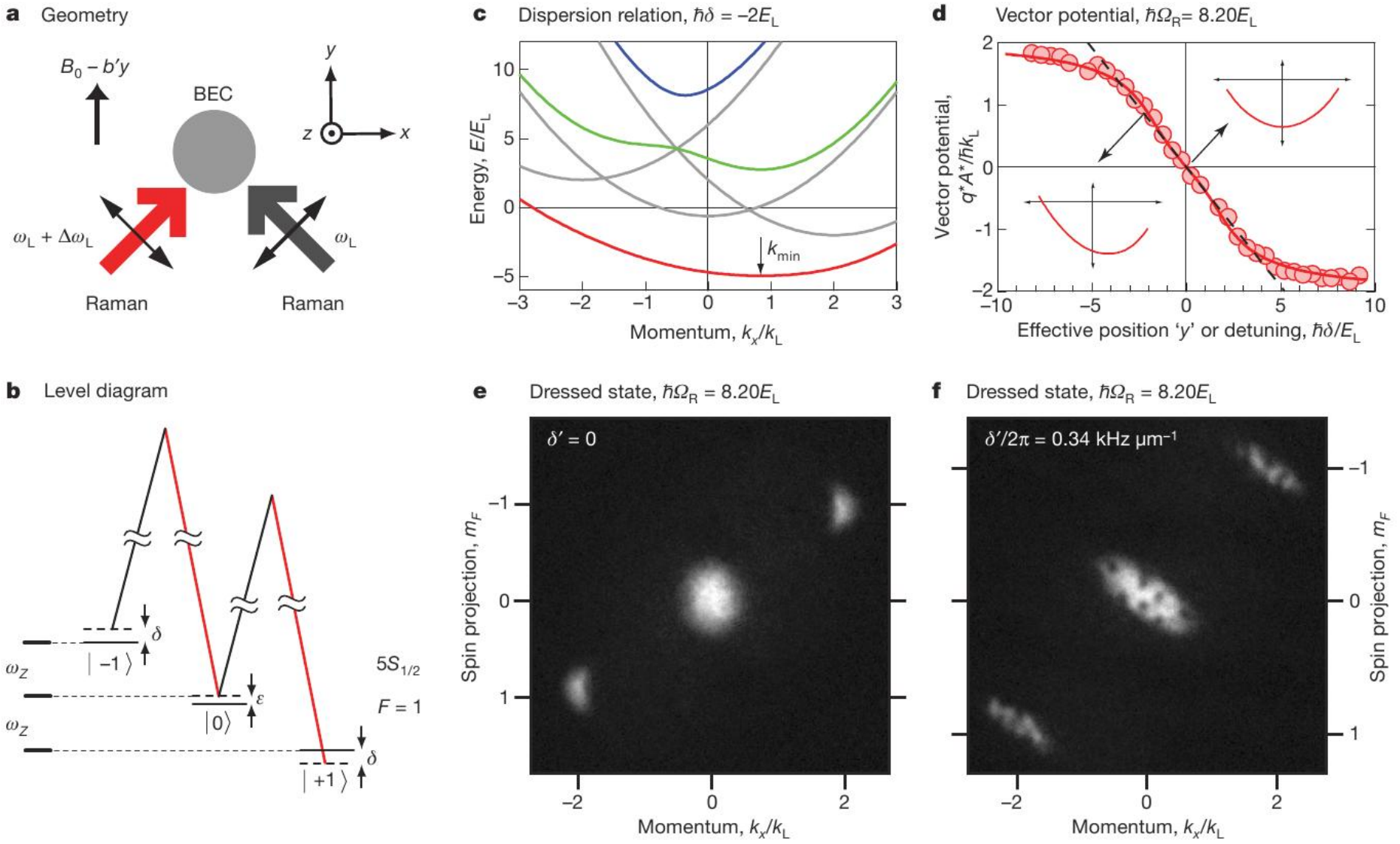

Figure 1 | Experiment summary for synthesizing magnetic fields. **a**, The BEC is in a crossed dipole trap in a magnetic field $B = (B_0 - b'y)\hat{y}$. Two Raman beams propagating along $\hat{y} \mp \hat{x}$ (linearly polarized along $\hat{y} \pm \hat{x}$) have frequencies ω_L and $\omega_L + \Delta\omega_L$. **b**, Raman coupling scheme within the $F = 1$ manifold: ω_Z and ε are the linear and quadratic Zeeman shifts, and δ is the Raman detuning. **c**, Energy–momentum dispersion relations. The grey curves represent the states without Raman coupling; the three coloured curves represent $E_j(k_x)$ of the dressed states. The arrow indicates the minimum at k_{min}. **d**, Vector potential $q^*A_x^* = \hbar k_{min}$ versus Raman detuning δ. The insets show the dispersion $E_1(k_x)$ for $\hbar\delta = 0$ (top inset) and $-2E_L$ (bottom inset). **e**, **f**, Dressed BEC imaged after a 25.1-ms TOF without (**e**) and with (**f**) a gradient. The spin components $m_F = 0$ and ± 1 separate along $\hat{y}$ owing to the Stern–Gerlach effect.